Rhenium–osmium and molybdenum isotope systematics of black shales from the Lower Cambrian Niutitang Formation, SW China: Evidence of a well oxygenated ocean at ca. 520 Ma

Lu Yin[a,b], Jie Li[a,c,*], Hui Tian[a], Xiaoping Long[d]

[a] State Key Laboratory of Isotope Geochemistry, Guangzhou Institute of Geochemistry, Chinese Academy of Sciences, Guangzhou 510640, China
[b] University of Chinese Academy of Sciences, Beijing 100049, China
[c] Institutions of Earth Science, Chinese Academy of Sciences, Beijing, 100029, China
[d] State Key Laboratory of Continental Dynamics, Department of Geology, Northwest University, Xi'an 710069, China

ARTICLE INFO

ABSTRACT

The Early Cambrian was a key period in Earth's history, and the reconstruction of ancient ocean chemistry on spatial and temporal scales can contribute to a better understanding of events during that period. New Early Cambrian data for Re–Os and Mo isotopic compositions and redox-sensitive elements (RSE) are reported here for the Niutitang Formation, SE Chongqin, SW China. A Re–Os age of 520 ± 30 Myr (Model 3, 2σ, $n = 21$, MSWD = 62) and a $(^{187}Os/^{188}Os)_i$ ratio of 0.79 ± 0.11 were obtained, consistent with previously reported data for equivalent strata from other areas. Separate regression of samples with $(^{187}Os/^{188}Os)_i$ of 0.72–0.79 and 0.81–0.89 produce more precise ages of 520.1 ± 9.5 Myr (Model1, 2σ, $n = 7$, MSWD = 1.0) and 513 ± 10 Myr (Model 1, 2σ, $n = 8$ MSWD = 0.96) respectively, suggesting heterogeneity in the primary source of Os as the dominant cause of scatter and uncertainty. High initial $^{187}Os/^{188}Os$ of 0.79 ± 0.11 may indicate a high Os input from oxidative weathering of upper continental crust for Early Cambrian ocean.

Based on RSE data such as Mo, U, V enrichment and Ni/Co, V/Cr, V/(V + Ni), Mo_{EF}/U_{EF}, Re/Mo ratios, two geochemically distinct zones (upper and lower) can be delineated in the sedimentary sequence, as reflected in drillcore sections. The upper section ($n = 9$) is characterized by low total organic carbon (TOC) contents (mean 1.8 ± 1.5 wt%), low RSE contents (Mo $(0.008 \pm 0.006) \times 10^{-3}$ g/g; V $(0.22 \pm 0.15) \times 10^{-3}$ g/g; U $(0.008 \pm 0.004) \times 10^{-3}$ g/g), and low V/Cr (2.0 ± 1.7), Ni/Co (5.9 ± 3.5), Mo_{EF}/U_{EF} (2.6 ± 1.8), and Mo/TOC (6.0 ± 3.9) ratios; in contrast, the lower core section ($n = 13$) is characterized by high TOC contents (4.4 ± 2.2 wt%), high RSE contents (Mo $(0.10 \pm 0.08) \times 10^{-3}$ g/g; V $(1.0 \pm 1.0) \times 10^{-3}$ g/g; U $(0.05 \pm 0.04) \times 10^{-3}$ g/g), high V/Cr (6 ± 5), Ni/Co (24 ± 14), Mo_{EF}/U_{EF} (6.3 ± 2.2), and Mo/TOC (21 ± 9) ratios (uncertainties are $\pm$ 1SD here). Significantly decreasing trends of those redox proxies from lower to upper sections suggest that the depositional conditions evolved from anoxic/euxinic to oxic condition. All samples display extremely low Re/Mo ratios of 0.2×10^{-3}–1.9×10^{-3}, indicating the absence of intermediate reducing conditions, possibly reflecting rapid ocean oxygenation.

The Mo isotopic composition in the sedimentary succession of the YC9 core exhibits a large variation, with $\delta^{98/95}Mo$ values of 0.04–2.00‰. Upper section $\delta^{98/95}Mo$ values display an opposite trend to Mn content and negative correlation with Mo/TOC ratios, indicating Mo fractionation associated with adsorption on Mn oxides or oxyhydroxides. Lower section $\delta^{98/95}Mo$ values are positively correlated with Mo/TOC ratios and negatively with Re/Mo ratios, suggesting incomplete conversion of molybdates to tetrathiomolybdates under weakly euxinic conditions.

High $\delta^{98/95}Mo$ of 2.00‰ and high average Mo/TOC ratios of 21 $(10^{-6}$ g/g)/wt% were observed in euxinic shales in the Niutitang Formation, suggesting extensive ocean oxygenation may have taken place at ca. 520 Ma.

* Corresponding author at: State Key Laboratory of Isotope Geochemistry, Guangzhou Institute of Geochemistry, Chinese Academy of Sciences, Guangzhou 510640, China.
E-mail address: jieli@gig.ac.cn (J. Li).

1. Introduction

The Ediacaran-Cambrian transition was a key period in Earth's history, as it recorded major changes in continental configuration, biological evolution, global climate, ocean geochemistry and redox conditions (Amthor et al., 2003; Berner et al., 2003; Landing, 2004; Guo et al., 2007; Schröder and Grotzinger, 2007). Some researchers proposed that widespread oxygenation of the deep ocean may have been the trigger for the evolution of the Ediacaran biota and the subsequent Cambrian Explosion (Fike et al., 2006; Canfield et al., 2007). However, it is still unclear when the widespread oceanic oxygenation took place. Sahoo et al. (2012) suggested an extensive ocean oxygenation at ca. 632 Ma, however, geochemical data from early and middle Ediacaran sedimentary successions are consistent with less oxygenated conditions, except following the ca. 580 Ma Gaskiers glaciation and at ca. 560–551 Ma (Canfield et al., 2007, 2008; McFadden et al., 2008; Li et al., 2010; Kendall et al., 2011; Johnston et al., 2012; Och and Shields-Zhou, 2012). Recently, extremely high $\delta^{98/95}$Mo ($\geq 2.00‰$) observed from the Lower Cambrian Niutitang Formation, South China, suggested that there may be additional episodes of extensive ocean oxygenation that took place during the Early Cambrian (Wille et al., 2008; Chen et al., 2015,; Kendall et al., 2015; Wen et al., 2015; Cheng et al., 2016). The Mo isotope composition of seawater can be used as a global tracer for ocean redox conditions, with heavier seawater Mo isotope composition indicating a more oxygenated global ocean (e.g. Anbar, 2004; Siebert et al., 2005; Pearce et al., 2008; Wille et al., 2008; Wen et al., 2009; Kendall et al., 2015). However, $\delta^{98/95}$Mo data from the Niutitang Formation are mostly lower than 2.00‰ (e.g. Lehmann et al., 2007; Wille et al., 2008; Dahl et al., 2011; Xu et al., 2012; Zhou et al., 2012, 2015; Chen et al., 2015; Kendall et al., 2015; Kurzweil et al., 2015; Wen et al., 2015; Cheng et al., 2016). These lower $\delta^{98/95}$Mo values may reflect a more deoxygenated global ocean state, or may be attributable to Mo isotopic fractionation in local depositional environments under weakly euxinic or non-euxinic conditions (Barling et al., 2001; Arnold et al., 2004; Poulson et al., 2006; Siebert et al., 2006; Neubert et al., 2008; Brucker et al., 2009; Feng et al., 2014; Kendall et al., 2017), or the operation of an Fe–Mn oxide shuttle (a process of being oxidized and precipitated of the dissolved Mn and Fe that has accumulated within the euxinic deep water; Scholz et al., 2013; Noordmann et al., 2015). The application of $\delta^{98/95}$Mo as a global ocean redox proxy may therefore need to take into consideration the influence of local redox conditions.

In previous studies, redox-sensitive-element (RSE, e.g. Mo, U, V) contents and their ratios (e.g. V/Cr, Ni/Co, and V/(V + Ni)) have been used to constrain the depositional conditions for the Niutitang Formation, with the results suggesting that the bottom water evolved from anoxic/euxinic conditions to oxic/suboxic conditions (e.g. Yang et al., 2004; Xu et al., 2012; Pi et al., 2013; Li et al., 2015; Wen et al., 2015; Cheng et al., 2016). However, these data may not reveal whether a Fe–Mn oxide shuttle process occurred, or whether the sulfide concentration in bottom water were high enough for quantitative MoS_4^{2-} formation and the capture of seawater-like $\delta^{98/95}$Mo values in sediments. Weakly euxinic conditions (H_2S concentration < 11 μM) and the Fe–Mn oxide shuttle process may be prevalent in continental margin basins, and sediments deposited under such conditions may exhibit variable $\delta^{98/95}$Mo values (Helz et al., 1996; Erickson and Helz, 2000; Poulson et al., 2006; Arnold et al., 2012). Additionally, most previous studies were based on samples from weathered outcrops, and isotopically light Mo can be adsorbed to residual phases during weathering (Archer and Vance, 2008; Pearce et al., 2010; Liermann et al., 2011; Siebert et al., 2015; Wang et al., 2015), which may result in low $\delta^{98/95}$Mo in sediments.

We here provide new RSE and Mo isotope data from a drillcore in the SE Chongqin area, SW China, and the covariant relationship between $\delta^{98/95}$Mo values and traditional local redox proxies (Mn content, V/Cr, Ni/Co, V/(V + Ni)) were investigated in the present study to explore possible causes of $\delta^{98/95}$Mo variations in the sediments. Re, U, and Mo contents and their ratios were also studied. Sediment data indicate that Re and U begin to be authigenically enriched in sediments at or just below the zone of Fe reduction, while excessive Mo precipitation occurs in the sulfide zone (Crusius et al., 1996; Crusius and Thomson, 2000); authigenic Mo uptake is strongly enhanced by the particulate Fe–Mn oxide shuttle (Crusius et al., 1996). Therefore, Mo/U and Re/Mo ratios may provide additional information about local redox conditions, especially regarding aqueous H_2S fluctuations and the operation of an Fe–Mn oxide shuttle.

Additionally, the ^{187}Re–^{187}Os isotope system has been used to constrain the depositional age of the Niutitang Formation in SE Chongqin area. The ^{187}Re–^{187}Os isotope system has been demonstrated to be a precise and accurate depositional geochronometer for black shales (Ravizza and Turekian, 1989; Singh et al., 1999; Creaser et al., 2002; Schaefer and Burgess, 2003; Selby and Creaser, 2003; Cohen, 2004; Cumming et al., 2012). Precise Re–Os isochron ages indicate that post-depositional processes have not affected the dated rock units (Jaffe et al., 2002; Kendall et al., 2009b; Rooney et al., 2012), allowing the confident application of tracers such as the Mo isotope proxy and RSEs. Moreover, initial ^{187}Os/^{188}Os ratios provide constraints on temporal variations in ^{187}Os/^{188}Os ratios in contemporary seawater (Ravizza and Turekian, 1989, 1992; Ravizza et al., 1991; Pegram et al., 1992; Cohen and Coe, 1999; Hannah et al., 2004; Ravizza and Paquay, 2008; Kendall et al., 2009a). The joint application of the Re–Os geochronometer and Mo isotope analysis therefore has the potential to constrain temporal variations in oceanic chemistry over geological time periods.

In general, the present study involved the investigation of RSE contents, and Re–Os and Mo isotopic systematics, for the Lower Cambrian Niutitang Formation in SE Chongqin, SW China. In this paper we: (1) present a new depositional Re–Os age for the Niutitang Formation and an estimation of the Os isotopic composition of Early Cambrian seawater; (2) reconstruct the local Early Cambrian depositional environment in SE Chongqin and the possible impact of aqueous H_2S fluctuations and Fe–Mn oxide shuttle processes on $\delta^{98/95}$Mo values of sediments; and (3) further our understanding of the oxygenation state of the Early Cambrian ocean.

2. Geological setting

The Yangtze Platform includes the Yangtze Block and Nanhua Basin. During the early Neoproterozoic Sibao Orogeny, the Yangtze and Cathaysia tectonic blocks collided, forming a coherent craton (Li et al., 2002). At *ca* 820 Ma, or possibly earlier (mid-Neoproterozoic), this craton started rifting, resulting in the formation of a failed intra-cratonic rift basin between the two blocks, which is called the Nanhua Basin (Wang and Li, 2003). The Nanhua Basin evolved from being a rift basin to a passive continental margin basin at *ca* 750–690 Ma (Wang and Li, 2003). Upper Ediacaran–Lower Cambrian strata in the Yangtze Platform comprise shallow carbonate platform facies, siliceous–argillaceous slope facies, and siliceous basin facies (Zhu et al., 2003; Goldberg et al., 2007). The carbonate platform was later flooded, with the formation of a deep sand–mud shelf as a result of large-scale transgression (Steiner et al., 2001), while the siliceous slope basin evolved into a muddy slope basin. The muddy shelf was later transformed into a carbonate platform (Feng et al., 2001).

The Niutitang Formation and equivalent strata are widely distributed in the slope-to-shelf region of the Nanhua Basin (Zhu et al., 2003) and overlie the Dengying Formation via a low-angle unconformity. The formation is dominated by black shales, with its lower part having a variable lithology with sedimentary phosphorite and barite units, and tens-of-meter thick "stone coal" (combustible shale) of algal origin. An organic- and sulfide-rich polymetallic ore layer a few centimeters thick is locally distributed in the lowermost part of the formation. Previous studies have suggested that the sedimentary sequence of this formation can be divided into chemically distinct upper

and lower zones. The lower zone is characterized by high total organic carbon (TOC) contents, and moderate to strong enrichment in RSEs (e.g., Mo, V, and U), while the upper zone exhibits lower TOC contents and less enrichment in RSEs (Xu et al., 2012; Pi et al., 2013; Wen et al., 2015; Cheng et al., 2016). Trace element contents and their ratios, coupled with Fe speciation, indicate that the lower Niutitang Formation was deposited under dominantly euxinic conditions and the upper part under suboxic/oxic conditions (Yang et al., 2004; Wang et al., 2012b; Xu et al., 2012; Wen et al., 2015; Cheng et al., 2016).

The depositional age of the Niutitang Formation is still debated. Re–Os dating of the sulfide-rich polymetallic ore layer has yielded regressions of 560 ± 50 Myr (Horan et al., 1994), 541 ± 16 Myr (Mao et al., 2002), 542 ± 11 Myr (Li et al., 2003), and 521 ± 5 Myr (Xu et al., 2011). Pb–Pb dating of black shales and the sulfide ore bed from the Niutitang Formation yielded ages of 531 ± 24 Myr and 521 ± 54 Myr, respectively (Jiang et al., 2006). Jiang et al. (2009) reported a U–Pb zircon age of 532.3 ± 0.7 Myr for an ash bed a few meters below the polymetallic Ni–Mo–PGE ore layer in the Zhongnancun section, Guizhou Province. Wang et al. (2012a) reported a SHRIMP U–Pb zircon age of 522.7 ± 4.9 Myr for an ash bed ~1 m below the Ni–Mo–PGE ore layer in the Taoying section, Guizhou Province.

3. Sampling and methods

Twenty-two rock samples of the Niutitang Formation were collected from Well YC9 drilled for shale gas exploration near Youyang County in SE Chongqin, which is located in the shelf-to-slope region of the Nanhua Basin (Fig. 1). The geographic coordinate is (108°55′ E, 28°23′ N). The sampling depth ranged from 1351.8 to 1465.7 m, and covered almost the entire sedimentary sequence of the Niutitang Formation. The depth of the boundary of Niutitang Formation and Dengying Formation is ~1475.3 m. The thickness of the Niutitang sequences in this section is about 115 m. The stratigraphic sequence is shown in Fig. 2. The drillcore was divided into sections of a few meters thickness. Samples from each section were crushed, and a split of ~5 g ground to ~200 mesh in an agate mill for trace element, TOC, and Re–Os and Mo isotope analysis.

All analyses were carried out at the State Key Laboratory of Isotope Geochemistry, Guangzhou Institute of Geochemistry (GIG), Chinese Academy of Sciences (CAS), Guangzhou, China.

Trace elements (V, Ni, Cr, Mn, Co) were analyzed by ICP–MS (Thermo Scientific™ iCAP™ RQ). Before analysis, the powders were ashed at 650 °C to remove organic matter, and digested in $HNO_3 + HF + HClO_4$ in Teflon pressure vessel to dissolve refractory minerals (Details in protocols described by Liu et al., 1996). Rhodium
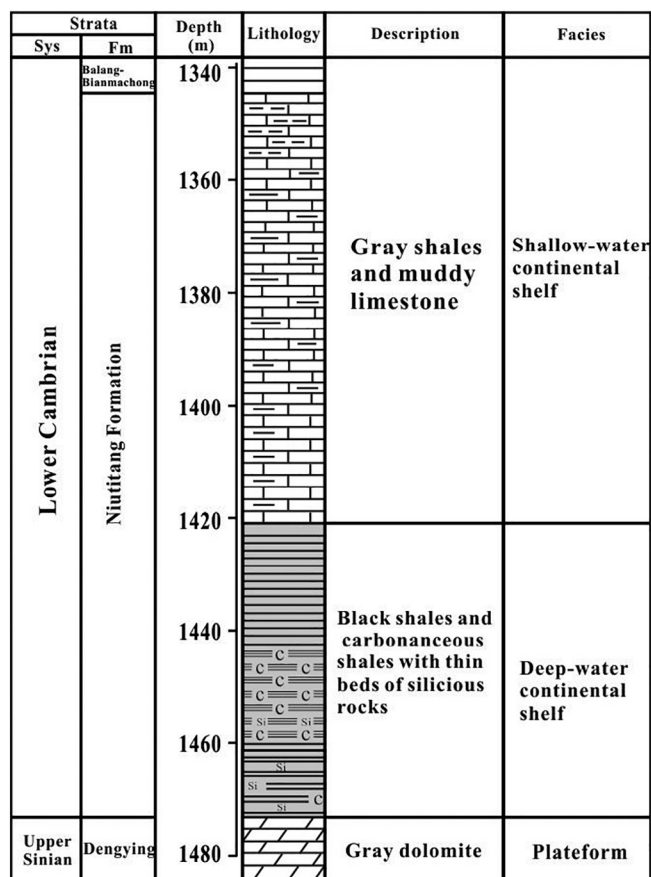

Fig. 2. Stratigraphic column showing the black shales in lower Cambrian strata from YC9 drillcore, SE Chongqin area.

was used as an internal standard to monitor and correct the signal drift of the instrument. Eight rock standards, including USGS G-2, W-2, MRG-1, and AGV-1, and Chinese national rock standards GSD-12, GSR-1, GSR-2, and GSR-3, were used for calibration. The analysis result for the international reference material BHVO-2 was consistent with the reference value within 5% analytical precision (Table 1, due to width limits on the page, the numerical values that reflect the uncertainty of trace elements analytical process were not listed in Table 1. These values can be seen in the Supplementary Table 1).

Mo contents and isotopic compositions of the black shales were determined by the double-spike method. Mo was separated and purified

Fig. 1. Simplified paleogeographic map of the Yangtze Platform during the Ediacaran–Cambrian transition, showing the three major facies under consideration here (modified from: Steiner et al., 2001; Wen et al., 2015).

Table 1

Mo isotope composition, TOC content, RSE enrichment and geochemical data for Niutitang Formation in drillcore YC9.

Samples	Depth (m)	Lithology	TOC wt%	V (10^{-6} g/g)	Cr (10^{-6} g/g)	Co (10^{-6} g/g)	Ni (10^{-6} g/g)	Mo (10^{-6} g/g)	U (10^{-6} g/g)	Mn (10^{-6} g/g)	Al$_2$O$_3$ wt%	Mo/TOC (10^{-6} g/g/wt%)	Ni/Co	V/Cr	V/(V + Ni)	Re/Mo (10^{-3})	Mo$_{EF}$	U$_{EF}$	V$_{EF}$	R$_{EF}$	Mo$_{EF}$/U$_{EF}$	δ$^{98/95}$Mo ‰
Upper core section																						
YC9-1	1351.8	Gray shale	0.5	164	214	19.7	179	4.1	4.5	642	17.6	8.1	9.1	0.8	0.48	0.1	4.4	1.5	1.3	0.5	2.9	0.18 ± 0.04
YC9-2	1369.9	Gray shale	0.3	178	116	23.7	67.5	2.0	4.5	356	20.8	6.0	2.8	1.5	0.73	0.2	1.8	1.3	1.2	0.5	1.4	0.33 ± 0.06
YC9-3	1395.0	Gray shale	0.8	172	96.5	21.1	73.6	11.3	7.6	434	17.5	15.1	3.5	1.8	0.70	0.3	12.2	2.6	1.3	3.4	4.7	0.29 ± 0.04
YC9-4	1406.7	Gray shale	3.3	206	104	20.9	74.9	19.7	9.8	139	17.7	5.9	3.6	2.0	0.73	0.5	21.0	3.4	1.6	10.9	6.2	0.15 ± 0.05
YC9-5	1410.9	Gray shale	0.3	172	201	18.7	172	1.5	4.3	467	20.3	6.0	9.2	0.9	0.50	0.2	1.4	1.3	1.1	0.3	1.1	0.54 ± 0.04
YC9-6	1411.3	Gray shale	1.7	105	147	12.3	138	6.6	8.8	554	11.0	3.9	11.2	0.7	0.43	0.3	11.4	4.9	1.3	4.0	2.3	1.14 ± 0.04
YC9-7	1413.0	Gray shale	3.0	181	93.6	20.1	64.9	10.9	12.0	201	7.1	3.7	3.2	1.9	0.74	0.4	28.8	10.3	3.4	13.0	2.8	1.00 ± 0.02
YC9-8	1414.6	Gray shale	4.3	178	87.9	23.3	53.3	9.4	15.7	191	14.9	2.2	2.3	2.0	0.77	0.7	11.9	6.4	1.6	9.1	1.9	0.66 ± 0.02
YC9-9	1424.4	Gray shale	2.1	598	97.0	28.1	231	6.8	47.6	352	15.5	3.3	8.2	6.2	0.72	0.6	8.3	18.7	5.2	5.2	0.4	1.27 ± 0.04
Lower core section																						
YC9-10	1428.6	Black shale	3.3	471	383	17.8	439	91.0	27.9	219	15.0	27.2	24.7	1.2	0.52	1.0	115.0	11.4	4.2	125	10.1	1.42 ± 0.02
YC9-11	1433.9	Black shale	2.5	221	98.7	24.7	89.8	25.4	14.4	253	16.3	10.0	3.6	2.2	0.71	0.2	29.5	5.4	1.8	7.6	5.5	2.00 ± 0.02
YC9-12	1436.2	Black shale	1.4	462	104	14.7	83.9	26.6	13.0	409	16.5	18.4	5.7	4.4	0.85	1.1	30.4	4.8	3.8	33.7	6.3	0.83 ± 0.04
YC9-13	1440.0	Black shale	2.0	486	92.8	16.5	91.0	37.0	15.7	425	14.6	18.3	5.5	5.2	0.84	1.1	48.0	6.6	4.5	56.8	7.3	1.16 ± 0.05
YC9-14	1443.7	Black shale	2.6	494	320	15.4	348	47.1	24.0	539	13.4	18.0	22.7	1.5	0.59	0.7	66.7	11.0	5.0	50.5	6.1	1.41 ± 0.02
YC9-15	1447.8	Black shale	4.5	142	602	19.3	600	94.6	6.0	327	16.7	20.9	31.1	0.2	0.19	0.6	106.8	2.2	1.1	63.1	48.5	1.28 ± 0.03
YC9-16	1451.0	Black shale	4.7	943	65.6	24.1	874	159	67.7	157	8.2	33.6	36.3	14.4	0.52	0.8	367.8	50.6	15.6	303	7.3	1.25 ± 0.02
YC9-17	1453.0	Black shale	7.2	1826	75.6	13.7	331	294	120	233	15.9	40.9	24.2	24.2	0.85	1.0	348.9	46.1	15.5	372	7.6	1.38 ± 0.02
YC9-18	1454.6	Black shale	8.5	1677	345	11.4	539	125	64.6	29.9	7.0	14.6	47.3	4.9	0.76	1.2	334.0	55.9	32.1	427	6.0	0.69 ± 0.02
YC9-19	1459.3	Black shale	5.9	850	273	13.2	445	98.2	94.3	173	13.3	16.8	33.6	3.1	0.66	1.3	140.1	43.4	8.7	194	3.2	1.05 ± 0.02
YC9-20	1462.3	Black shale	6.0	3439	299	16.1	259	105	34.6	39.3	7.7	17.6	16.1	11.5	0.93	1.9	257.7	27.4	60.4	506	9.4	0.04 ± 0.04
YC9-21	1463.8	Black shale	2.7	2062	193	7.3	130	28.2	33.5	18.7	12.2	10.4	17.8	10.7	0.94	1.6	43.9	16.8	22.9	72	2.6	0.13 ± 0.05
YC9-22	1465.7	Black shale	6.2	487	510	18.	768	157	105	51.5	11.1	25.5	41.6	1.0	0.39	0.2	267.2	58.0	5.9	66	4.6	1.62 ± 0.02
BHVO-2				321	278	44.0	116		0.41	1270												

Note: Mo$_{EF}$, V$_{EF}$ and U$_{EF}$ were calculated following the formula: X$_{EF}$ = (X/Al)$_{sample}$/(X/Al)$_{PAAS}$, where X = Mo, V or U. We applied a detritus correction assuming PAAS concentrations of 1 × 10^{-6} g/g Mo, 3.1 × 10^{-6} g/g U, 140 × 10^{-6} g/g V and 18.9 wt% Al$_2$O$_3$, respectively (all values from Taylor and McLennan, 1985). R$_{EF}$ and U$_{EF}$ were calculated following the formula: X$_{EF}$ = (X/Al)$_{sample}$/(X/Al)$_{UCC}$, assuming UCC concentrations of 0.4 × 10^{-9} g/g Re, 0.05 × 10^{-9} g/g Os and 8.0 wt% Al$_2$O$_3$, respectively.

by ion-exchange chromatography using BPHA resin, and analyzed by MC–ICP–MS (Thermo-Fisher Scientific Neptune Plus). Procedures and instrument parameters are described by Li et al. (2014). The isotopic composition of Mo is expressed as $\delta^{98/95}$Mo relative to NIST SRM 3134. The double-spike and normalizing standard (NIST SRM 3134) was calibrated following the procedure of Siebert et al. (2001) and Zhao et al. (2016). NIST SRM 3134 standard solution and IAPSO seawater were repeatedly measured during the sample analyses. The $\delta^{98/95}$Mo values of NIST SRM 3134 and IAPSO seawater were determined to be 0.00 ± 0.06‰ (2 SD, $n = 20$) and 2.04 ± 0.09‰ (2 SD, $n = 4$), respectively, consistent with certified values and those reported previously (Greber et al., 2012; Pearce et al., 2009). The Mo procedural blank was < 0.1 ng, and much less than the total Mo in the samples. Nägler et al., 2014 suggested setting the $\delta^{98/95}$Mo value of NIST SRM 3134 to +0.25‰ to facilitate the use of canonical values, such as +2.3‰ for seawater, in comparing old and future data. Values of $\delta^{98/95}$Mo relative to NIST SRM 3134 (0.25‰) were calculated as follows:

$$\delta^{98/95}\text{Mo}(‰) = \left(\frac{(\delta^{98/95}\text{Mo})_{sample}}{(\delta^{98/95}\text{Mo})_{NIST3134} * 0.99975} - 1 \right) * 1000$$

Re and Os contents and Os isotopic ratios were determined by isotope dilution coupled with ICP–MS for Re, and TIMS for Os. In previous studies, Re and Os analyses of organic-rich whole-rock powders involved *aqua regia* digestion in Carius tubes at 230 °C for 24 h (Cohen and Coe, 1999; Creaser et al., 2002), resulting in dissolution of the entire rock matrix with the exception of quartz and some feldspar. However, Re–Os isotopic chronometry of black shales is based on Re and Os predominantly scavenged from seawater during sediment deposition, and any non-hydrogenous Re and Os could have diverse ^{187}Re/^{188}Os and ^{187}Os/^{188}Os ratios, which may affect accuracy and precision (Selby and Creaser, 2003). To minimize any non-hydrogenous Re and Os, a more suitable digestion procedure described in Yin et al. (2017), was applied in the present study, as follows. Black shale powder (0.2–0.5 g) (without ashing at 650 °C) was digested together with a ^{185}Re–^{190}Os tracer in 12 mL of a H_2O_2/HNO_3 solution (2 mL 12 M HNO_3 plus 10 mL 30% H_2O_2) in a Carius tube at 220 °C for 24 h. Analytical methods followed protocols described by Li et al. (2013, 2015) and Yin et al. (2017). Total procedural blanks for Os and Re were 0.8 ± 0.2 pg (2 SD, $n = 6$) with an average ^{187}Os/^{188}Os ratio of 0.1289 ± 0.0048, and 8 ± 3 pg (2 SD; $n = 6$), respectively. Blank contributions were typically < 2% for Re and < 5% for Os. Regression analyses were performed using Isoplot v. 3.0 (Ludwig, 2003) with a ^{187}Re decay constant of 1.666×10^{-11} yr^{-1} (Smoliar et al., 1996). Total uncertainties include measurement, blank, decay constant, and spike calibration uncertainties, and are reported at the 2σ level, with the associated rho error correlation function (Kendall et al., 2004).

4. Results

4.1. TOC and trace element data

TOC and trace element data are presented in Table 1, with stratigraphic trends shown in Fig. 3. The YC9 core can be divided into two geochemically distinct sections.

Black shales from the lower core section are characterized by high TOC contents (1.4–8.5 wt%) and moderate to high abundances of RSEs such as Mo ((0.025–0.29) $\times 10^{-3}$ g/g; mean (0.10 $\pm$ 0.08) $\times 10^{-3}$ g/g), V ((0.14–3.44) $\times 10^{-3}$ g/g; mean (1.0 $\pm$ 1.0) $\times 10^{-3}$ g/g), U ((0.006–0.12) $\times 10^{-3}$ g/g; mean (0.05 $\pm$ 0.04) $\times 10^{-3}$ g/g), Re ((0.006–0.30) $\times 10^{-6}$ g/g; mean (0.09 $\pm$ 0.08) $\times 10^{-6}$ g/g), Ni ((0.08–0.54) $\times 10^{-3}$ g/g; mean (0.38 $\pm$ 0.26) $\times 10^{-3}$ g/g), and Cr ((0.065–0.60) $\times 10^{-3}$ g/g; mean (0.26 $\pm$ 0.17) $\times 10^{-3}$ g/g). Uncertainties are $\pm$ 1 SD here and throughout the text, unless otherwise specified. Their Mn contents have a wide range of

(0.019–0.54) $\times 10^{-3}$ g/g. Mo/TOC ((10^{-6} g/g)/wt%) ratios have a range of 10–40 with an average value of 21 $\pm$ 8, which are similar to those of anoxic sediments from the semi-restricted modern Cariaco Basin (mean 25 $\pm$ 5; Algeo and Lyons, 2006). V/(V + Ni), V/Cr, Ni/Co, Mo$_{EF}$/U$_{EF}$, and Re/Mo ratios have respective ranges (and means) of 0.19–0.94 (0.7 $\pm$ 0.2), 0.2–24.2 (6 $\pm$ 5), 3.6–47.3 (24 $\pm$ 14), 2.6–48.5 (6.3 $\pm$ 2.2), and (0.2–1.9) $\times 10^{-3}$ ((1.0 $\pm$ 0.5) $\times 10^{-3}$) (Table 1). Black shales from the upper core section exhibit much lower TOC (0.2–4.2 wt%) and RSE contents: Mo (0.004–0.019) $\times 10^{-3}$ g/g (mean (0.008 $\pm$ 0.006) $\times 10^{-3}$ g/g); V (0.11–0.60) $\times 10^{-3}$ g/g (mean (0.22 $\pm$ 0.15) $\times 10^{-3}$ g/g); U (0.004–0.048) 10^{-3} g/g (mean (0.008 $\pm$ 0.004) $\times 10^{-3}$ g/g); Re (0.3–9.8) $\times 10^{-9}$ g/g (mean (3.5 $\pm$ 3.2) $\times 10^{-3}$ g/g); Ni (0.05–0.23) $\times 10^{-3}$ g/g (mean (0.12 $\pm$ 0.06) $\times 10^{-3}$ g/g); and Cr (0.09–0.21) $\times 10^{-3}$ g/g (mean (0.13 $\pm$ 0.05) $\times 10^{-3}$ g/g). Their Mn contents are relatively high at (0.19–0.64) $\times 10^{-3}$ g/g. Overall, Mo/TOC ratios are significantly lower than in the lower section, with values of 3.2–15.1 (average 6.1 $\pm$ 7). Trace element ratios such as V/(V + Ni), V/Cr, Ni/Co, Mo$_{EF}$/U$_{EF}$, and Re/Mo have respective ranges (and means) of 0.48–0.77 (0.64 $\pm$ 0.13), 0.7–6.2 (2.0 $\pm$ 1.6), 2.3–11.2 (5.9 $\pm$ 3.4), 0.4–6.2 (2.6 $\pm$ 1.8), and (0.1–0.7) $\times 10^{-3}$ ((0.4 $\pm$ 0.2) $\times 10^{-3}$).

In general, TOC, Mo, V, U, Re, Ni, and Cr contents, and V/Cr, Ni/Co, V/(V + Ni), Re/Mo, Mo$_{EF}$/U$_{EF}$, and Mo/TOC ratios exhibit a significant decreasing trend from the lower to upper sections, whereas the Mn content increases (Fig. 3; Table 1).

4.2. Mo isotopes

Black shale $\delta^{98/95}$Mo values vary from +0.04 to +2.00‰ (Fig. 4; Table 1) with an overall average of 0.90 $\pm$ 0.55‰ ($n = 22$). The upper core section exhibits relatively low values of 0.18–1.27‰ (average 0.62 $\pm$ 0.42‰), while lower core section values range from +0.04 to +2.00‰ (average 1.10 $\pm$ 0.56‰). Most samples from the lower section have values of > 1.0‰, with lower values of 0.04–1.05‰ occurring at depths of 1463.8–1546.6 m. The $\delta^{98/95}$Mo values in the Niutitang Formation exhibit two decreasing trends and an increasing trend with depth (Fig. 4), decreasing abruptly from 1.62 to 0.04‰ as depth decreases from 1465.7 m to 1462.3 m, and then increasing from 0.04 to 2.00‰ at depth of 1462.3 to the boundary between upper and lower boundary, and decreasing in the upper section from 2.00 to 0.18‰ (Fig. 4). The $\delta^{98/95}$Mo trend in the lower section is consistent with that observed in similar zones in the Zunyi profile, Guizhou Province (Xu et al., 2012; Fig. 4).

4.3. Re–Os isotopic compositions

Variations in Re and Os contents in the sequence are similar to those of Mo (Table 2; Fig. 4), with values being higher in the lower core section ((6.2–297) $\times 10^{-9}$ g/g Re and (0.68–6.59) $\times 10^{-9}$ g/g Os, respectively) and much higher than average continental crustal values (Re 0.2–2 $\times 10^{-9}$ g/g; Os 0.03–0.05 $\times 10^{-9}$ g/g; Esser and Turekian, 1993; Crusius et al., 1996; Peucker-Ehrenbrink and Jahn, 2001; Hattori et al., 2003), indicating a dominantly hydrogenous origin. Re and Os contents are much lower in the upper core section, with (0.3–9.8) $\times 10^{-9}$ g/g Re and (0.09–0.53) $\times 10^{-9}$ g/g Os.

The Niutitang Formation samples exhibit large variations in ^{187}Re/^{188}Os and ^{187}Os/^{188}Os ratios from 17.3–460.2 and 0.4–4.7, respectively. Linear regression analysis of the Re–Os data yielded a Model-3 age of 538 $\pm$ 49 Myr with (^{187}Os/^{188}Os)$_i$ ratio of 0.69 $\pm$ 0.18 (2σ, $n = 22$, MSWD = 132; Fig. 5a). Excluding the anomalous sample YC9-9 (Fig. 5b), a Re–Os age of 520 $\pm$ 30 Myr and (^{187}Os/^{188}Os)$_i$ ratio of 0.79 $\pm$ 0.11 (2σ, $n = 21$, MSWD = 62) is obtained.
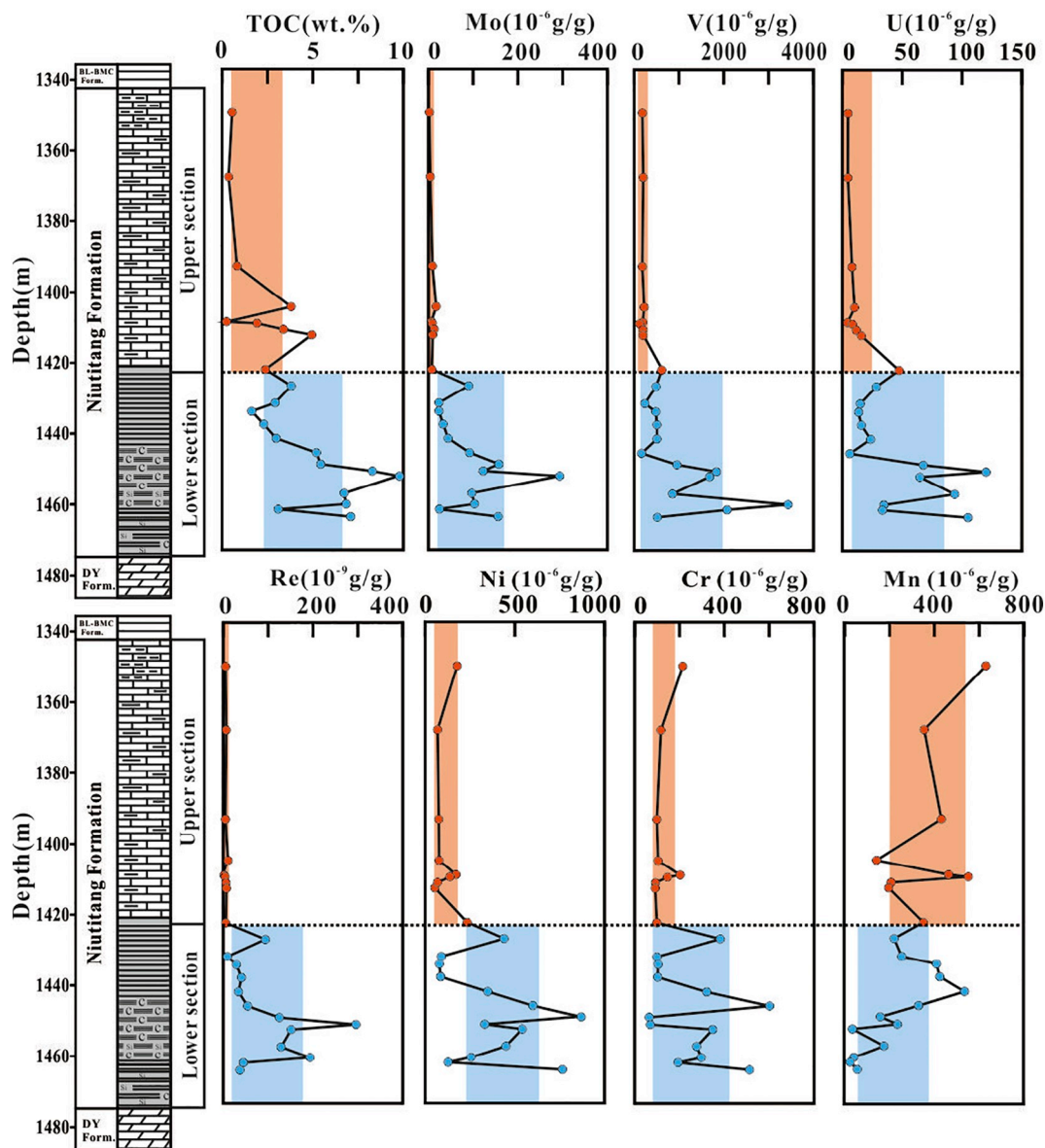
Fig. 3. Stratigraphic distribution of TOC contents and trace elements. The blue shaded area represents the average value of the lower core section, and the orange area is the average value of the upper core section. (For interpretation of the references to colour in this figure legend, the reader is referred to the web version of this article.)

5. Discussion

5.1. Re–Os geochronology of Black shales of the Niutitang Formation

The 520 ± 30 Myr age calculated by regression analysis of Re–Os data for core YC9 (excluding sample YC9-9) is consistent with recent Re–Os (521 ± 5 Myr) and U–Pb (522.7 ± 4.9 Myr) ages for equivalent strata in Guizhou Province (Xu et al., 2011; Wang et al., 2012a). Sample YC9-9 exhibits a significant deviation from the regression line, indicating a disturbance of the Re–Os system in this sample. The large MSWD value of 62 associated with the regression age on all 22 samples implies that the scatter about the linear correlation line is controlled by geological factors, rather than analytical uncertainties (Ludwig, 2003). It is considered here that heterogeneity in the primary source of Os is the dominant cause of scatter and uncertainty. The residence time of dissolved Os in present day seawater is about 10^3–10^4 years (Oxburgh, 1998; Peucker-Ehrenbrink and Ravizza, 2000). This value may be even lower under conditions of a predominantly anoxic atmosphere and ocean or in a stratified ocean with oxidizing surface waters and suboxic,

anoxic or euxinic deep waters, allowing rapid changes in the seawater Os isotopic ratio. To assess the variability of $(^{187}Os/^{188}Os)_i$ ratios, the individual sample isotope compositions were back-calculated using the ^{187}Re decay constant of 1.666×10^{-11} yr^{-1} (Smoliar et al., 1996), and using the age determined from the regression (Table 2). The calculated initial ratios at 520 Ma have a range of 0.47–1.03 (except sample YC9-9, which has a ratio of −0.13). The samples were divided according to the calculated $(^{187}Os/^{188}Os)_i$ ratios into four subsets of 0.46–0.55, 0.72–0.79, 0.81–0.89, and 0.92–1.03, with regression analysis producing a Model-3 age of 527 ± 180 Myr (2σ, $n = 3$, MSWD = 15), Model-1 age of 520.1 ± 9.5 Myr (2σ, $n = 7$, MSWD = 1.0), Model-1 age of 513 ± 10 Myr (2σ, $n = 8$ MSWD = 0.96), and Model-3 age of 489 ± 390 Myr (2σ, n = 3, MSWD = 16), respectively (Fig. 6). Samples with $(^{187}Os/^{188}Os)_i$ ratios of 0.46–0.55 and 0.92–1.03 gave highly imprecise Re–Os ages, attributable to the low number of samples ($n = 3$). Ages of samples with ratios of 0.72–0.79 and 0.81–0.89 are identical within uncertainty. The relatively precise ages for these two subsets argue against any post-depositional disturbance of the Re–Os system (such as hydrocarbon maturation, weathering, or hydrothermal
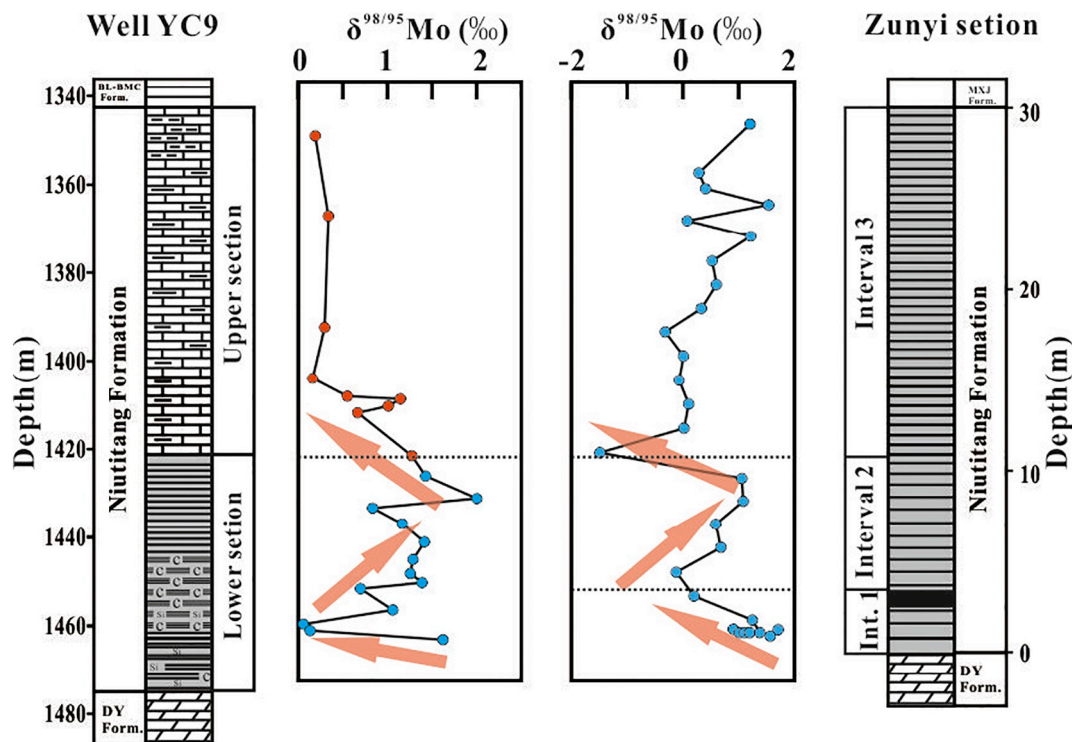
Fig. 4. Stratigraphic distribution of $\delta^{98/95}$Mo values in the Niutitang Formation (Well YC9; this study) and Zunyi section (Xu et al., 2012). $\delta^{98/95}$Mo in lower section of YC9 exhibit similar trends to that in Interval 1 and 2 of the profile in Zunyi section.

processes; Ravizza and Turekian, 1989; Cohen and Coe, 1999; Creaser et al., 2002; Crusius and Thomson, 2000), and indicate that stratigraphic variability is the principal controlling factor in the degree of scatter.

Initial ^{187}Os/^{188}Os ratios in organic-rich sediments are considered to record the seawater Os isotopic composition at the time of deposition (e.g. Ravizza and Turekian, 1989; Ravizza et al., 1991; Ravizza and Turekian, 1992; Pegram et al., 1992; Peucker-Ehrenbrink et al., 1995;

Pegram and Turekian, 1999; Ravizza et al., 2001; Cohen and Coe, 2002, 2007; Ravizza and Peucker-Ehrenbrink, 2003; Cohen, 2004). Major sources of Os in seawater include volcanism (Alves et al., 1999), weathering of young subduction arc-related crust (Martin et al., 2000), hydrothermal metasomatism at mid-ocean spreading centers (Ravizza et al., 1996; Sharma et al., 2000; Pierson-Wickmann et al., 2002; Cave et al., 2003), dissolution of cosmic dust (Peucker-Ehrenbrink, 1996), and riverine input from oxidative weathering and erosion of upper

Table 2
Re–Os isotope data for the YC9 drillcore from the Niutitang Formation.

Sample	Re (10^{-9} g/g)	2SE	Os (10^{-9} g/g)	2SE	^{187}Re/^{188}Os	2SE	^{187}Os/^{188}Os	2SE	Rho	(^{187}Os/^{188}Os)$_i$
Upper core section										
YC9-1	0.64	0.05	0.188	0.006	17.3	3.3	0.619	0.011	0.10	0.47
YC9-2	0.50	0.02	0.085	0.003	32.0	6.5	1.136	0.027	0.07	0.86
YC9-3	2.98	0.06	0.170	0.005	102.2	8.7	1.732	0.021	0.07	0.84
YC9-4	9.76	0.11	0.499	0.014	115.6	5.5	1.866	0.008	0.09	0.86
YC9-5	0.32	0.02	0.130	0.004	12.7	3.2	0.660	0.011	0.06	0.55
YC9-6	2.19	0.04	0.243	0.007	49.1	4.8	1.150	0.010	0.04	0.72
YC9-7	4.67	0.08	0.333	0.010	80.3	5.4	1.582	0.010	0.04	0.88
YC9-8	6.80	0.08	0.530	0.015	73.5	4.1	1.576	0.006	0.05	0.94
YC9-9	4.07	0.11	0.330	0.010	61.6	4.6	0.409	0.003	0.02	−0.13
Lower core section										
YC9-10	93.64	1.59	1.944	0.055	332.1	7.7	3.436	0.005	0.03	0.55
YC9-11	6.24	0.07	0.681	0.020	52.0	3.0	1.485	0.005	0.10	1.03
YC9-12	27.96	0.26	0.701	0.020	265.8	7.7	3.064	0.010	0.17	0.75
YC9-13	41.62	0.40	1.049	0.030	264.0	6.5	3.055	0.007	0.12	0.76
YC9-14	33.85	0.80	1.274	0.036	162.5	5.6	2.198	0.005	0.03	0.78
YC9-15	53.06	0.98	1.647	0.047	207.8	5.7	2.729	0.004	0.02	0.92
YC9-16	124.08	2.39	3.362	0.096	242.6	5.8	2.928	0.003	0.02	0.82
YC9-17	297.44	2.73	6.593	0.197	314.3	5.2	3.550	0.005	0.06	0.82
YC9-18	151.37	2.19	3.658	0.104	278.8	5.4	3.185	0.005	0.05	0.76
YC9-19	129.35	2.43	2.406	0.068	403.2	9.4	4.401	0.007	0.04	0.89
YC9-20	195.35	1.72	3.270	0.093	460.2	6.7	4.725	0.005	0.14	0.72
YC9-21	44.01	1.60	1.082	0.031	275.1	11.7	3.230	0.007	0.02	0.84
YC9-22	36.70	2.53	1.307	0.037	173.0	12.6	2.268	0.004	0.01	0.76

Note: 'Rho': the associated error correlation (Ludwig, 2003). '(^{187}Os/^{188}Os)$_i$': initial ^{187}Os/^{188}Os ratios calculated at 520 Ma using λ of 1.666 e^{-11} year^{-1} (Smoliar et al., 1996). '2SE': double of Standard Error, determined by the uncertainties of measurement, blank, the ^{187}decay constant and the spike calibrations.
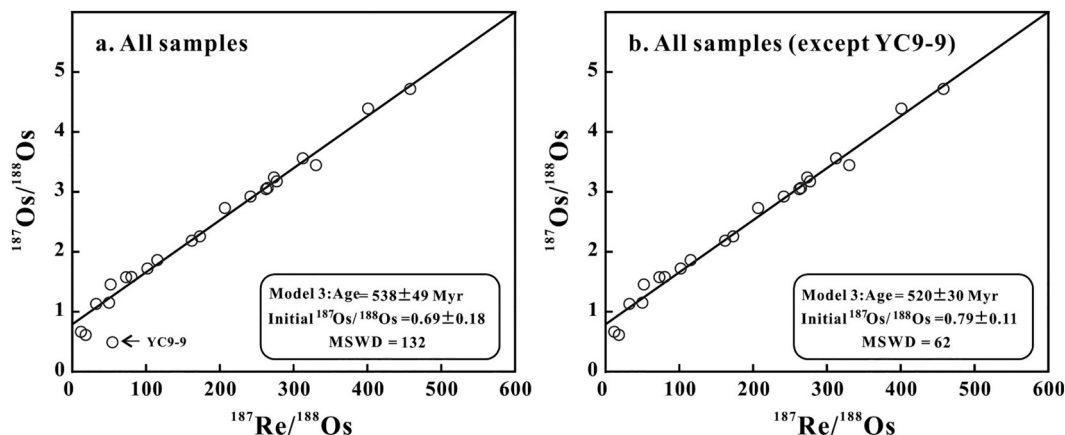
Fig. 5. Re–Os isochron diagrams for the YC9 core samples: (a) all samples; (b) all samples except YC9-9, which exhibits a significant deviation from the regression line.

continental crust (Peucker-Ehrenbrink, 1996). Variations of seawater ^{187}Os/^{188}Os may result from major changes in the proportion of radiogenic Os and unradiogenic Os delivered to the oceans (Peucker-Ehrenbrink et al., 1995; Levasseur et al., 1999; Pegram and Turekian, 1999; Ravizza et al., 2001; Cohen and Coe, 2002, 2007; Ravizza and Peucker-Ehrenbrink, 2003; Cohen, 2004; Dubin and Peucker-Ehrenbrink, 2015).

The seawater residence time of Os in past predominantly anoxic or stratified ocean was probably lower than that in present well oxygeanted ocean. Additionally, Paquay and Ravizza (2012) reported that the Os isotope composition in seawater may not have been homogenous during the Late Pleistocene glaciations. Thus, preservation of intital Os

isotope composition in organic rich sediments may just reflect local seawater. Nevertheless, some intersting insights can be gained from the initial Os isotope data of ancient organic rich sedimenatry rocks (Ravizza and Esser, 1993; Kendall et al., 2009a). For instance, for a predominantly anoxic Archaean atmosphere and oceans, riverine transport of soluble Re and radiogenic Os from weathering and erosion of crustal rocks would be negligible, resulting in deposition of Archaean with chondritic or near-chondritic initial ^{187}Os/^{188}Os ratios (e.g. Hannah et al., 2004; Anbar et al., 2007; Yang et al., 2009). In contrast, moderate or radiogenic initial ^{187}Os/^{188}Os values were achieved from organic rich sediments of Late Neoproterozoic (e.g. Kendall et al., 2004, 2006, 2009a), suggesting that crustal Os fluxes from rivers may exert a
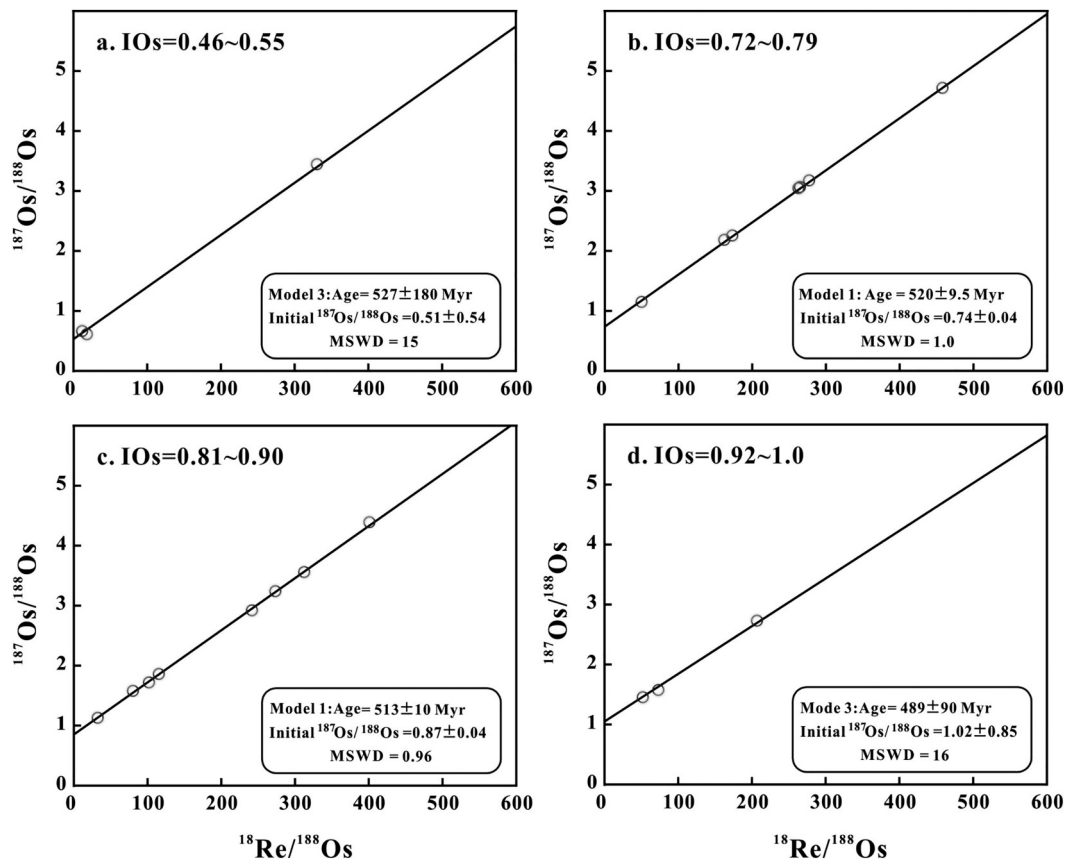

Fig. 6. Separate regression analyses of samples with (^{187}Os/^{188}Os)$_i$ ratios of (a) 0.46–0.55, (b) 0.72–0.79, (c) 0.81–0.90, and (d) 0.92–1.00. (^{187}Os/^{188}Os)$_i$ ratios were back-calculated using the ^{187}Re decay constant of 1.666×10^{-11} yr^{-1} (Smoliar et al., 1996), and the age determined from the regression on all samples.

significant control on the $^{187}Os/^{188}Os$ isotope composition of seawater. For the YC9 core, the initial $^{187}Os/^{188}Os$ ratio determined from Re–Os isochron regression is 0.79 ± 0.11, which is within the range of initial ratios determined from Re–Os isochron regression of Late Neoproterozoic organic rich sediments (0.62–1.24, Kendall et al., 2004, 2006, 2009a) and much higher than those ratios from Archaean organic rich sediments, which may suggest a high Os input from oxidative weathering of upper continental crust during Early Cambrian.

5.2. Redox interpretations for Niutitang shales in the YC9 core

Previous studies have indicated that the Niutitang Formation black shale sequence in South China was deposited during a gradual evolution from anoxic/euxinic to oxic conditions (e.g. Goldberg et al., 2007; Li et al., 2010, 2012; Xu et al., 2012; Wang et al., 2012b; Pi et al., 2013; Wu et al., 2014; Wen et al., 2015; Zhang et al., 2017). The sequence displayed in the YC9 core exhibits multiple redox conditions, which can be identified according to RSE characteristics.

Redox sensitive elements (e.g. Mo, V, U and Re) are conservative or quasi-conservative under oxic conditions (Calvert and Pedersen, 1993; Orberger et al., 2003; Algeo and Maynard, 2004; Rimmer, 2004; Tribovillard et al., 2006), and their concentrations in shales deposited from an oxic water column are commonly similar to crustal values (except for sediments very rich in Fe–Mn oxyhydroxides) (Emerson and Huested, 1991; Morford et al., 2009; Miller et al., 2011). Anoxic shales capture dissolved Mo, V, U and Re from seawater much more effectively than oxic shales (e.g. Vine and Tourtelot, 1970; Holland, 1979; Algeo and Maynard, 2004; Rimmer, 2004; Tribovillard et al., 2006). High Mo, V, U and Re contents thus provide evidence of anoxic depositional environments in an open basin. Authigenic enrichments of Mo, U, V and Re in the Niutitang Formation were investigated through calculation of "enrichment factors" (EF):

$$X_{EF} = (X/Al)_{sample}/(X/Al)_{PAAS}$$

where X and Al are element-X and Al contents (wt%), respectively. Samples are normalized to post-Archean Australia average shale (PAAS) compositions of Taylor and McLennan (1985) for Mo_{EF}, U_{EF} and V_{EF}, and normalized to upper Continental Crust (UCC) compositions of Esser and Turekian (1993) for Re_{EF}.

Lower section samples exhibit high authigenic enrichment of Mo ($Mo_{EF} = 29–349$) and Re ($Re_{EF} = 7.6–505$), and moderate to high enrichment of V and U ($U_{EF} = 4.8–58$; $V_{EF} = 1.8–60$; Table 1; Fig. 7), suggesting a dominantly anoxic depositional environment. Upper section samples exhibit much lower enrichments ($Mo_{EF} = 1.4–29$; $U_{EF} = 1.3–19$; $V_{EF} = 1.1–5.2$; $Re_{EF} = 0.5–10$; Table 1; Fig. 7). Low enrichment values from any particular stratigraphic unit have a less definitive meaning because they could reflect multiple scenarios, including strong basin restriction in an oxygenated ocean (Algeo and Lyons, 2006), low enrichment in oxic/suboxic local environments (Emerson and Huested, 1991; McManus et al., 2006), or low dissolved concentrations in a poorly oxygenated ocean (Dahl et al., 2011; Kendall et al., 2015). However, observations from regional stratigraphic studies and the distribution of small shell fossils (SSFs) indicate that the Early Cambrian Nanhua Basin was well connected with the open ocean (Zhu et al., 2003, 2013; Jiang et al., 2011; Jin et al., 2014). Furthermore, isochron regression of the Niutitang Formation black shales yield much higher $(^{187}Os/^{188}Os)_i$ ratios compared to Archaean sediments, arguing against a predominantly anoxic atmosphere and ocean (Section 5.1). It follows that the low Mo, U, V and Re enrichments calculated for the upper section may not be attributable to low dissolved concentrations due to basin restriction or low oxygenation, but rather to an oxic or suboxic local environment.

V/(V + Ni), Ni/Co, and V/Cr ratios have proved to be useful proxies in reflecting local depositional redox conditions (Dill, 1986; Hatch and Leventhal, 1992; Jones and Manning, 1994; Rimmer, 2004). A Ni/Co ratio of < 5 is indicative of oxic conditions, 5–7 of dysoxic conditions,

and > 7 of suboxic to anoxic conditions; a V/Cr ratio of < 2 indicates oxic conditions, 2–4.25 of dysoxic conditions, and > 4.25 of suboxic to anoxic conditions (Jones and Manning, 1994). Hatch and Leventhal (1992) compared V/(V + Ni) ratios with other geochemical redox indicators (such as degree of pyritization) and concluded that V/(V + Ni) > 0.84 is indicative of euxinic conditions, 0.54–0.82 of anoxic conditions, and 0.46–0.60 of dysoxic conditions. For the Niutitang shales, Ni/Co and V/Cr ratios exhibit a significant decreasing trend from the lower to upper section (Fig. 8), with most samples in the lower section having Ni/Co > 7 and V/Cr > 4.25, reflecting dominantly anoxic conditions; and upper section samples having lower ratios reflecting suboxic or oxic conditions. The case for V/(V + Ni) ratios is not so straightforward, with the lower section (0.19–0.93, average 0.67 ± 0.22) not displaying ratios significantly higher than the upper section (0.48–0.77, average 0.64 ± 0.13). However, samples with V/(V + Ni) > 0.84 occur only in the lower section, indicating euxinic depositional conditions there.

Authigenic Mo–U covariation has proved useful in indicating redox conditions and processes in marine depositional systems (e.g., Algeo and Tribovillard, 2009; Xiang et al., 2017). Under anoxic conditions, authigenic U uptake occurs at the Fe(II)/Fe(III) redox boundary, while authigenic Mo is enriched in the sulfate zone (Helz et al., 1996; Morford et al., 2009). For the open ocean, higher authigenic Mo/U ratios thus represent more reducing conditions. In plots of U_{EF} vs Mo_{EF}, the Niutitang black shales display a well-defined pattern of $Mo_{EF}–U_{EF}$ covariation similar to that of the modern unrestricted marine environment (Fig. 9; Algeo and Tribovillard, 2009). Lower section samples are characterized by high Mo_{EF} and U_{EF} values and high Mo_{EF}/U_{EF} ratios (2.6–49; mean 9.6), while the upper section exhibits lower Mo_{EF} and U_{EF} values, and much lower Mo_{EF}/U_{EF} ratios (0.4–6.2; mean 2.6). This is consistent with $Mo_{EF}–U_{EF}$ patterns observed in other equivalent formations (Cheng et al., 2016; Wen et al., 2015), indicating that the depositional environment evolved to more oxic conditions upward from the lower to upper core sections. Authigenic Mo uptake also occurs via the particulate Fe–Mn oxide shuttle (Crusius et al., 1996) with a rate substantially exceeding that of authigenic U uptake, resulting in higher Mo_{EF}/U_{EF} ratios and a steeper Mo_{EF} vs U_{EF} trend (Fig. 9; Wen et al., 2015). For the Niutitang black shales, Mo_{EF}/U_{EF} ratios linked to the Mn–Fe oxide shuttle can reach to more than five times that of seawater molar Mo/U ratios (present-day seawater Mo/U (weight ratio) = ~3.1, Algeo and Tribovillard, 2009). For the YC9 core, however, data for almost all samples of the lower section plot near the normal unrestricted marine Mo/U trend (Fig. 9), possibly indicating that Fe–Mn oxides shuttle process did not play a significant role in Mo enrichment in this area.

Rhenium adsorption occurs on Mn oxide and Fe oxyhydroxide surfaces, with its accumulation in sediments apparently being due solely to the degree of reducing conditions (Crusius et al., 1996; Crusius and Thomson, 2000; Morford et al., 2005). The coupling of authigenic Re and Mo sediment contents may therefore aid in distinguishing between intermediate reducing conditions and oxic/anoxic conditions. Low sediment Re/Mo ratios are indicative of deposition from oxic or euxinic bottom water, due to the potential for Mo adsorption on Mn oxides and the almost complete removal of dissolved Mo from sulfide bottom water, whereas high ratios indicate intermediate reducing conditions. Turgeon and Brumsack (2006) found that Re/Mo ratios in intermediate reducing (suboxic) sediments were as high as 15×10^{-3}. YC9 core samples display extremely low ratios of 0.2×10^{-3}–1.9×10^{-3}, indicating the absence of intermediate reducing depositional conditions (Fig. 10).

It is concluded that the lower core section was deposited under dominantly euxinic conditions, while the upper section was deposited under oxic conditions with an absence of intermediate reducing conditions, possibly reflecting rapid ocean oxygenation.
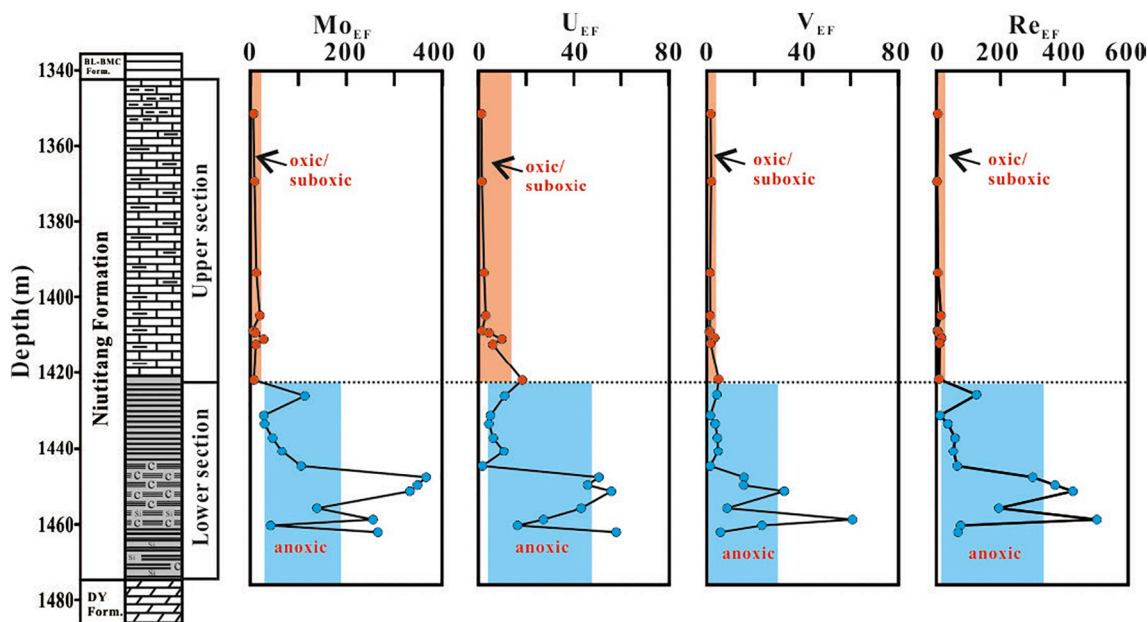
Fig. 7. The depositional environment inferred from Mo_{EF}, U_{EF}, V_{EF} and Re_{EF} values. The blue shaded area represents the average value of the lower core section, and the orange area is the average value of the upper core section. (For interpretation of the references to colour in this figure legend, the reader is referred to the web version of this article.)
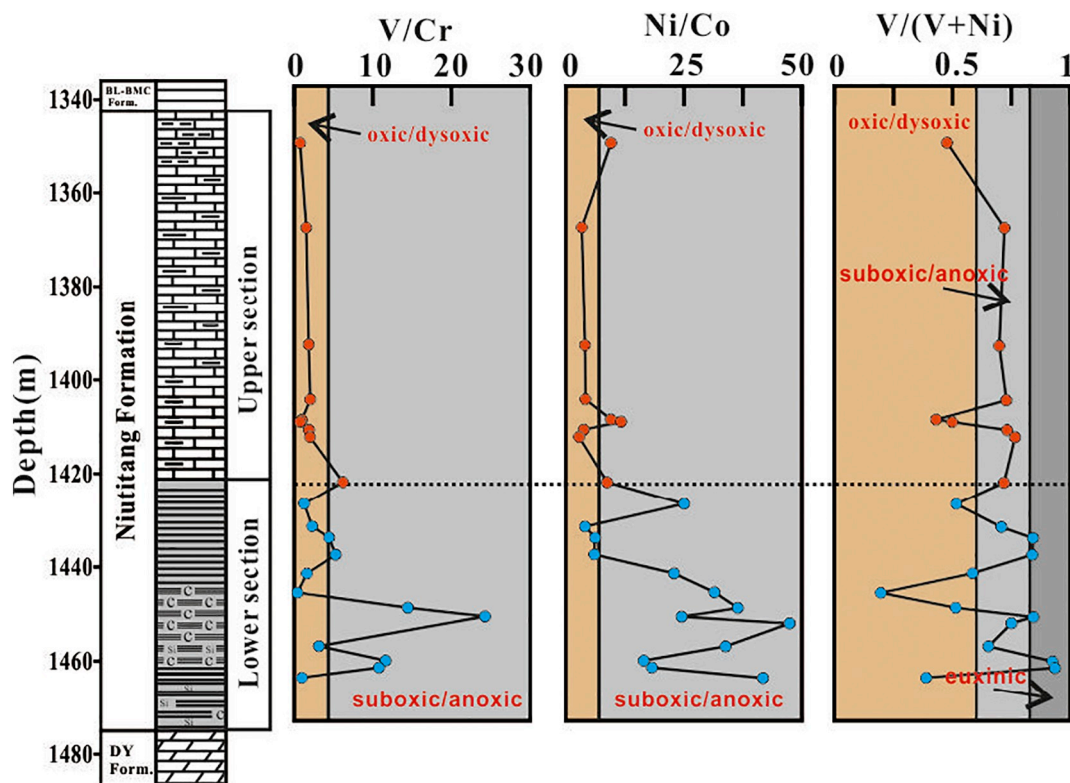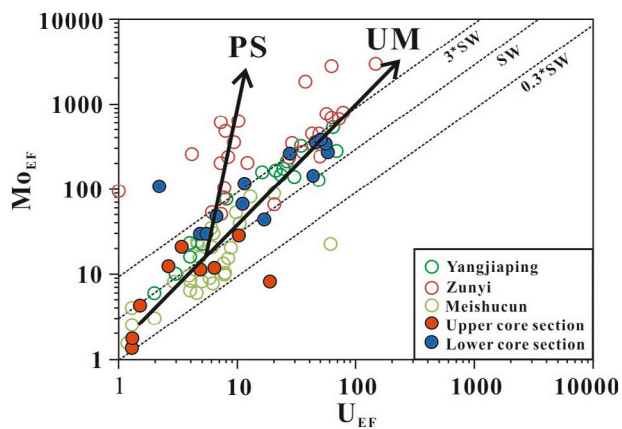

Fig. 8. The depositional environment inferred from V/Cr, Ni/Co, and V/(V + Ni) ratios. Boundaries for Ni/Co and V/Cr are from Jones and Manning (1994). The boundary for V/(V + Ni) is from Hatch and Leventhal (1992).

5.3. Interpretation of Mo isotope variations in the Niutitang shales
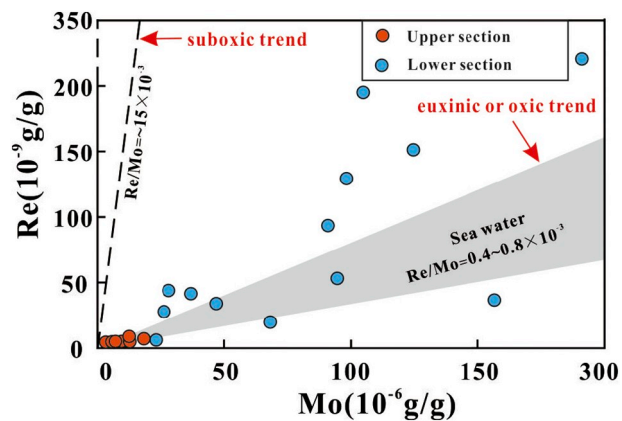
Mo isotope fractionation is known to occur under oxic/suboxic conditions, with only euxinic sediments recording prevailing seawater isotope compositions (Barling et al., 2001; Siebert et al., 2003; Barling and Anbar, 2004; Brucker et al., 2009). However, Mo fractionation is also observed in sediments where bottom waters are weakly euxinic

(aqueous H_2S concentration < 11 µM) or have experienced Fe–Mn oxide shuttle processes (Barling et al., 2001; Arnold et al., 2004; Poulson et al., 2006; Siebert et al., 2006; Neubert et al., 2008; Brucker et al., 2009). The application of Mo isotopes in assessing the Early Cambrian seawater oxygenation may therefore need to take into account the possible causes of Mo fractionation in sediments.

Black shales of the Niutitang Formation display a remarkable

Fig. 9. Plots of Mo_{EF} vs U_{EF}. The data shown are for Niutitang shales from Well YC9 and correlative units from multiple other sections of the Yangtze Block (Data of Zunyi and Meishucun is from Wen et al., 2015; data of Yangjiaping is from Cheng et al., 2016). 'UM' represents the 'unrestricted marine' trend. 'PS' represents the 'particulate shuttle' trend. Authigenic Mo uptake is accelerated strongly by the particulate Fe–Mn oxide shuttle, resulting in an increased Mo/U ratio and steeper Mo_{EF} vs U_{EF} trend. Samples from interval 1 of Zunyi section represent Mo_{EF}/U_{EF} ratios more than three times of the seawater molar ratio, which may reflect a particulate Fe–Mn oxide shuttle process (Wen et al., 2015). The diagonal lines represent multiples (0.3, 1, and 3) of the Mo/U ratio of present-day seawater, with an average weight ratio of 3.1 (Algeo and Tribovillard, 2009).

Fig. 10. Plots of Re vs Mo contents. The dashed line represents the possible Re/Mo ratio in suboxic conditions (Turgeon and Brumsack, 2006). The shaded area represents the possible seawater Re/Mo range (Crusius et al., 1996; Turgeon and Brumsack, 2006).

variation in Mo isotopic compositions with $\delta^{98/95}$Mo values of 0.04–2.00‰. The upper core section, deposited under oxic/suboxic conditions as described above, generally exhibits lower $\delta^{98/95}$Mo values (0.18–1.27‰). $\delta^{98/95}$Mo in this section display generally opposite trends to Mn content (Fig. 11), reflecting Mo fractionation controlled by Mo adsorption on Mn oxides or oxyhydroxide under oxic/suboxic conditions, as further indicated by the negative correlation between $\delta^{98/95}$Mo and Mo/TOC ratios and roughly positive correlation between $\delta^{98/95}$Mo and Re/Mo (Fig. 12). Fe–Mn oxides tend to enrich sediments in lighter Mo isotopes (Barling et al., 2001; Siebert et al., 2003; Barling and Anbar, 2004; Brucker et al., 2009), with samples containing more Fe–Mn oxides thus exhibiting higher Mo enrichment and lighter $\delta^{98/95}$Mo values.

RSEs are highly enriched in the lower core section with high V/Cr, Ni/Co, V/(V + Ni), and Mo_{EF}/U_{EF} ratios, and low Re/Mo ratios, indicating an euxinic depositional environment. Samples from this section exhibit a relatively elevated average $\delta^{98/95}$Mo value of

1.10 ± 0.56‰, but with a large variation. Mo isotopic compositions in euxinic sediments may be affected by Fe–Mn oxide shuttle processes (Scholz et al., 2013; Noordmann et al., 2015) or low aqueous H_2S concentrations (Barling et al., 2001; Arnold et al., 2004; Poulson et al., 2006; Siebert et al., 2006; Neubert et al., 2008; Brucker et al., 2009), as discussed here.

In a less-restricted continental margin basin, the redoxcline occurs in the water column where deep-water renewal is fast enough to sustain the Fe–Mn oxide shuttle. Frequent flushing with oxygenated seawater may have a significant impact on sediment $\delta^{98/95}$Mo values due to the formation of Fe–Mn oxides and their reductive dissolution in anoxic sediments (Scholz et al., 2013; Noordmann et al., 2015). Samples from near the top of the lower section (from YC9-17 to YC9-10), have Mn contents of (0.22–0.54) × 10^{-3} g/g, similar to samples deposited under oxic conditions (upper section: 0.19–0.64 × 10^{-3} g/g; Fig. 11), possibly indicating a Fe–Mn oxide shuttle process occurred during deposition of this section. However, samples with lower Mn contents exhibit relatively light $\delta^{98/95}$Mo values (Fig. 11, e.g. YC9-18, YC9-20, and YC9-21; Table 1), contrary to the hypothesis that the Fe–Mn shuttle played a dominant role in defining $\delta^{98/95}$Mo trends. Furthermore, Wen et al. (2015) suggested that authigenic Mo uptake can be accelerated by a particulate Fe–Mn oxide shuttle, causing euxinic sediments deposited under such conditions to have higher Mo_{EF}/U_{EF} ratios and steeper Mo_{EF}-U_{EF} trends. However, the YC9 lower section samples do not exhibit such high Mo_{EF}/U_{EF} ratios and steeper Mo_{EF}-U_{EF} trends (Fig. 9), suggesting that there may have been little contribution from a Fe–Mn oxide shuttle to Mo enrichment. In addition, samples from the lower core section exhibit a significantly positive relationship between Mo/TOC ratios and $\delta^{98/95}$Mo values (Fig. 12). It is known that Fe–Mn oxides tend to enrich lighter Mo isotopes, so if reductive dissolution of Fe–Mn oxide controlled $\delta^{98/95}$Mo trends, those euxinic samples would have higher Mo enrichment but lower $\delta^{98/95}$Mo values. It is therefore considered here that the $\delta^{98/95}$Mo variation in the lower core section was not controlled by a Fe–Mn oxide shuttle process.

Alternatively, $\delta^{98/95}$Mo variation may be attributable to incomplete conversion of molybdates to tetrathiomolybdates under weakly euxinic (H_2S concentration < 11 μM) conditions (Arnold et al., 2004; Nägler et al., 2005; Neubert et al., 2008; Dahl et al., 2011; Noordmann et al., 2015). On studying previously published $\delta^{98/95}$Mo data of euxinic samples from Lower Cambrian units (ca. 529–514 Ma) of the Nanhua Basin, Cheng et al. (2016) found that only 3.8% have $\delta^{98/95}$Mo values above 2.0‰, with most having values of 0–2.0‰, and concluded that relatively low aqueous H_2S concentrations may have been prevalent in euxinic waters there throughout the Early Cambrian. However, there is no viable proxy to distinguish which sediments deposited under weakly euxinic conditions, considering that those sediments may display similar signatures to those deposited under strongly euxinc condition, such as high Fe_{HR}/Fe_T and Fe_{PY}/Fe_{HR} (e.g. Kendall et al., 2015; Cheng et al., 2016). There is evidence of a positive correlation between aqueous H_2S concentrations and sediment $\delta^{98/95}$Mo values under weakly euxinic conditions (Nägler et al., 2005; Neubert et al., 2008; Arnold et al., 2012). It follows that the proxies reflecting the H_2S concentrations may co-vary with $\delta^{98/95}$Mo values under weakly euxinic conditions. In the plots of $\delta^{98/95}$Mo vs. local redox proxies such as Ni/Co, V/Cr, V/(V + Ni), Mo_{EF}/U_{EF}, Mo/TOC, and Re/Mo ratios (Fig. 13), $\delta^{98/95}$Mo values display no significant correlation with Ni/Co, V/Cr, V/(V + Ni), or Mo_{EF}/U_{EF} ratios, but have a roughly positive relationship with Mo/TOC and a well negative correlation with Re/Mo. This may suggest that $\delta^{98/95}$Mo fractionation in the lower section is controlled by H_2S, and Mo/TOC and Re/Mo can better reflect aqueous H_2S concentrations. The positive relationship between Mo/TOC and $\delta^{98/95}$Mo suggests that high aqueous H_2S concentration favor deposition of Mo as MoS_4^{2-}, thus increasing the marine sink of Mo. The linear correlation between Re/Mo and $\delta^{98/95}$Mo (with R^2 of 0.8) may suggest that Re/Mo may better reflect the conversion efficiency of dissolved MoO_4^{2-} and diminish the effect of fluctuation of the marine Mo inventory.
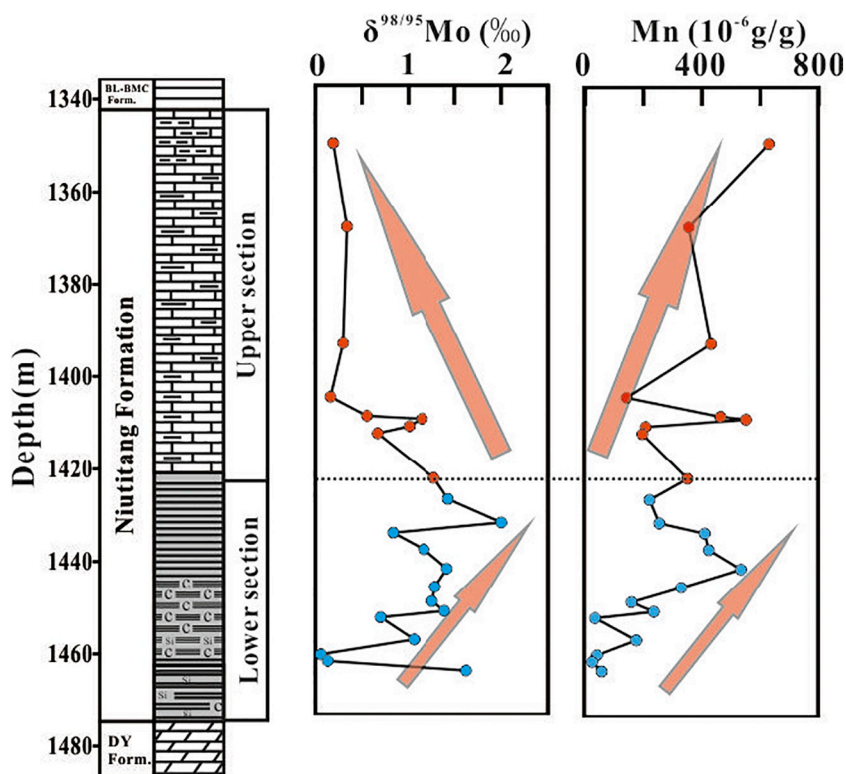
Fig. 11. Stratigraphic variation of $\delta^{98/95}$Mo and Mn content. Upper section samples display opposite trends between $\delta^{98/95}$Mo and Mn content, indicating processes of Mo adsorption onto Fe–Mn oxides which tend to enrich sediments in lighter Mo isotopes; Lower section samples display correlated trends between $\delta^{98/95}$Mo and Mn content, arguing against the operation of the Fe–Mn oxide shuttle.
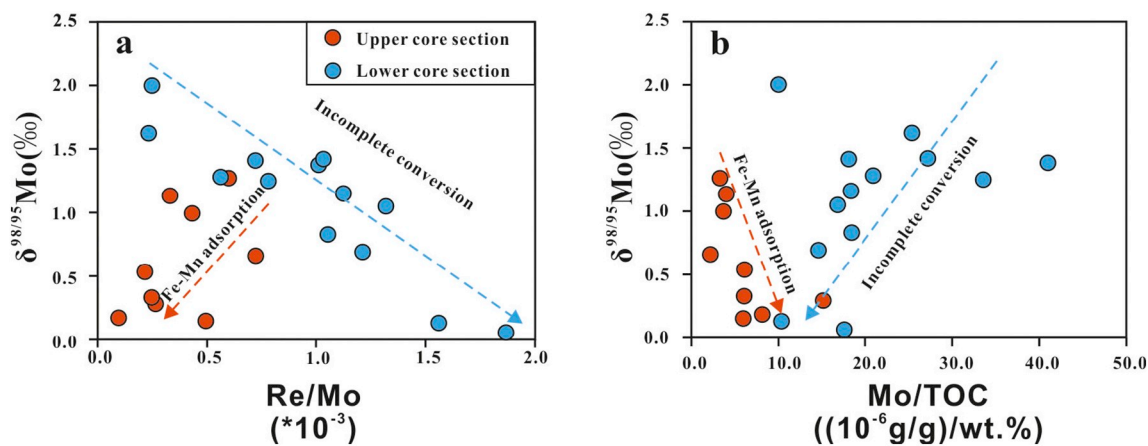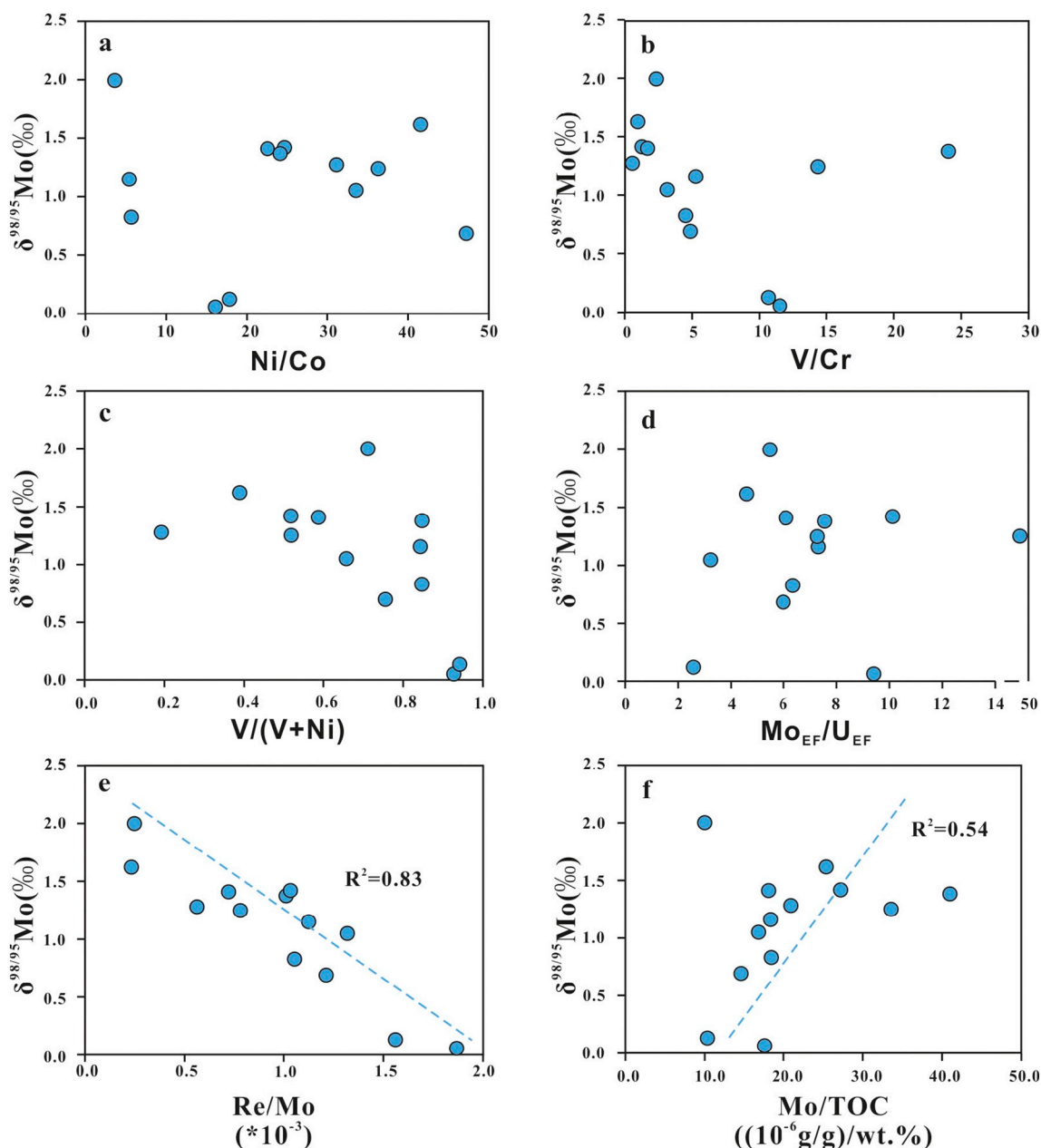

Fig. 12. Plots of $\delta^{98/95}$Mo vs (a) Re/Mo and (b) Mo/TOC. The upper core section shows a roughly positive correlation between $\delta^{98/95}$Mo and Re/Mo, and negative correlation between $\delta^{98/95}$Mo and Mo/TOC, indicating Mo isotope fractionation is controlled by processes of Mo adsorption onto Fe–Mn oxides (red line). The lower core section shows significantly negative correlation between $\delta^{98/95}$Mo and Re/Mo, and positive correlation between $\delta^{98/95}$Mo and Mo/TOC, suggesting Mo isotope fractionation is linked to incomplete conversion of MoO_4^{2-} to MoS_4^{2-} under weakly euxinic condition (blue line). (For interpretation of the references to colour in this figure legend, the reader is referred to the web version of this article.)

In summary, the Mo isotope fractionation in the upper section may be associated with Mo adsorption onto Mn oxides or oxyhydroxides, and Mo isotope fractionation in the lower section is linked to incomplete conversion of MoO_4^{2-} under weakly euxinic condition.

5.4. Implications for oceanic oxygenation during the early Cambrian

Local redox proxies indicate that the Early Cambrian seawater of the Nanhua Basin evolved from anoxic to oxic conditions (Goldberg et al., 2007; Wen et al., 2011; Xu et al., 2012; Pi et al., 2013; Wen et al., 2015; this study), but this does not necessarily mean that this is a global trend. The long oceanic residence time of Mo (400–800 kyr; Emerson and Huested, 1991; Miller et al., 2011) relative to the ocean mixing time (1–1.5 kyr) of the modern ocean allows $\delta^{98/95}$Mo values in an open
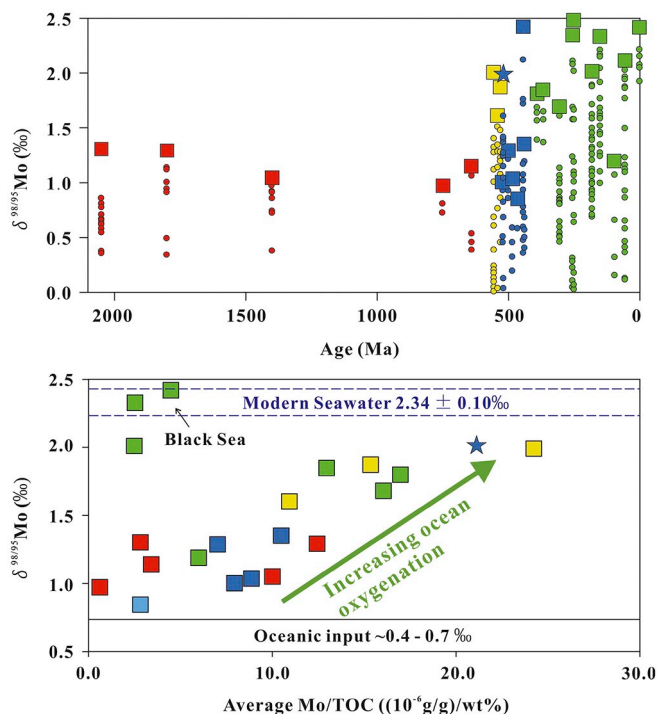
basin, or even in a moderately restricted basin, to track global values (Sahoo et al., 2012). The oceanic Mo isotope budget depends on the relative proportions of oxic and euxinic sinks. For example, the modern ocean is enriched in heavy Mo isotopes ($\delta^{98/95}$Mo = 2.34 ± 0.10‰; Barling et al., 2001; Siebert et al., 2003; Nägler et al., 2014) relative to oceanic inputs (dominated by rivers with an average $\delta^{98/95}$Mo value of ~0.7‰; Archer and Vance, 2008). The degree of heavy Mo enrichment depends largely on Mo adsorption on Fe–Mn oxides in oxygenated waters, with this process tending to enrich light Mo isotopes, resulting in significant isotopic fractionation (~3‰; Barling et al., 2001; Siebert et al., 2003; Barling and Anbar, 2004; Brucker et al., 2009). In contrast, Mo fractionation is often less significant (typically ≤1‰) during Mo burial in low-O_2 (< 10 μM) and anoxic marine environments where H_2S is present in pore and/or bottom waters (Barling et al., 2001; Arnold

Fig. 13. Plots of $\delta^{98/95}$Mo vs local redox proxies in lower core section: (a) Ni/Co; (b) V/Cr; (c) V/(V + Ni); (d) Mo$_{EF}$/U$_{EF}$; (e) Re/Mo; (f) Mo/TOC. Only Re/Mo ratios represent significantly linear correlation with $\delta^{98/95}$Mo (the blue stippled line, R^2 = 0.83). Mo/TOC ratios represent a roughly positive relationship with $\delta^{98/95}$Mo (R^2 = 0.54, eliminating three plots deviate the regression line). Ni/Co, V/Cr, V/(V + Ni) and Mo$_{EF}$/U$_{EF}$ show none correlation with $\delta^{98/95}$Mo. (For interpretation of the references to colour in this figure legend, the reader is referred to the web version of this article.)

et al., 2004; Poulson et al., 2006; Siebert et al., 2006; Neubert et al., 2008; Brucker et al., 2009). Heavier seawater Mo isotopic compositions thus generally reflect more oxygenated oceanic conditions, while low seawater $\delta^{98/95}$Mo values indicate extensive anoxia (Siebert et al., 2005; Wille et al., 2007; Pearce et al., 2008; Wen et al., 2009; Kendall et al., 2010). This principle is further supported by the findings in weakly euxinic environments. Sediments deposited under euxinic conditions can have $\delta^{98/95}$Mo that is up to 3.0‰ lower than seawater because of the incomplete conversion of MoO$_4^{2-}$ to MoS$_4^{2-}$ and preservation of Mo isotope fractionation during the formation of intermediate MoS$_x$O$_{4-x}^{2-}$ (Arnold et al., 2004, 2012; Neubert et al., 2008; Dahl et al., 2010), however, Mo burial fluxes to sediments in this condition are 2–3 orders of magnitude higher relative to oxic condition (Scott and Lyons, 2012; Brucker et al., 2009). Hence, widespread weakly euxinic oceans will not generate both high Mo/TOC and high

$\delta^{98/95}$Mo in anoxic sediments. Dahl et al. (2010) and Kendall et al. (2015) compiled $\delta^{98/95}$Mo and Mo/TOC data from organic rich mud rocks formed since the end of the Great Oxidation Event, and suggested that these rocks tend to have higher $\delta^{98/95}$Mo and higher average Mo/TOC with increasing ocean oxygenation (Fig. 14). Low $\delta^{98/95}$Mo and moderate Mo/TOC between 2050 and 640 Ma point to a generally moderately sized oceanic Mo reservoir that reflects a combination of pervasive oxidative weathering and redox-stratified oceans. High Mo/TOC (~23 (10^{-6} g/g)/wt%) and high $\delta^{98/95}$Mo (2.00‰) are also observed near the top of the Doushantuo Formation, indicating extensive ocean oxygenation at ca. 551 Ma (Kendall et al., 2015). Lower $\delta^{98/95}$Mo and lower Mo/TOC at 520–440 Ma may suggest a return to generally less oxygenated deep oceans with expanded sulfidic marine environments (Dahl et al., 2010; Zhou et al., 2012). High $\delta^{98/95}$Mo and high Mo/TOC after 390 Ma indicates a widespread and persistent ocean

Fig. 14. Temporal records of the $\delta^{98/95}$Mo and associated average Mo/TOC data from euxinic ORM, since the end of the Great Oxidation Event (Kendall et al., 2015, plus the $\delta^{98/95}$Mo and average Mo/TOC from drillcore YC9 black shales). Squares represent the highest $\delta^{98/95}$Mo for that time, Star represents the highest $\delta^{98/95}$Mo in samples from drillcore YC9, other data represented by small circles (red: > 640 Ma, orange: 555–530 Ma; blue: 520–440 Ma; green: 390–0 Ma). (a) Records of the highest $\delta^{98/95}$Mo from euxinic ORM over the past 2050 Ma. (b) Plot of the average Mo/TOC ratio versus the highest $\delta^{98/95}$Mo. Data sources: Barling et al., 2001; Arnold et al., 2004; Lehmann et al., 2007; Wille et al., 2008; Neubert et al., 2008; Pearce et al., 2008, 2010; Gordon et al., 2009; Kendall et al., 2009b, 2011; Dahl et al., 2010; Dickson and Cohen, 2012; Dickson et al., 2012; Herrmann et al., 2012; Zhou et al., 2012; Asael et al., 2013; Proemse et al., 2013; Westermann et al., 2014; Kendall et al., 2015; this study. (For interpretation of the references to colour in this figure legend, the reader is referred to the web version of this article.)

oxygenation. In this study, high average Mo/TOC (21 (10^{-6} g/g)/wt%) and high $\delta^{98/95}$Mo (highest value of 2.00‰) are observed in the lower section of the Early Cambrian Niutitang Formation, and indicate that extensive ocean oxygenation took place at ca. 520 Ma.

6. Conclusions

Re–Os isotope data for the lower stratigraphic section of black shales of the Niutitang Formation from SE Chongqin have a Re–Os age of 520 ± 30 Myr with an initial ^{187}Os/^{188}Os ratios of 0.79 ± 0.11 (2σ, $n = 21$, MSWD = 62). Separate regression of samples with initial ^{187}Os/^{188}Os ratios of 0.72–0.79 and 0.81–0.90 yields precise Re–Os ages of 520 ± 9.5 Myr (2σ, $n = 7$, MSWD = 1.0) and 513 ± 10 Myr (2σ, $n = 8$, MSWD = 0.96), respectively. These ages are consistent with those determined in previous studies by different methods, indicating that stratigraphic variation in initial ^{187}Os/^{188}Os ratios controlled the scatter in the regression. Initial ^{187}Os/^{188}Os ratios of ~0.79 determined from isochron regression of Early Cambrian Niutitang Formation are comparable to the values determined from organic rich sediments at ca. 657~ ca. 551 Ma and the ^{187}Os/^{188}Os value of present well oxygenated ocean, and is much higher than those values determined from Archaean organic rich sediments, suggesting a high Os input from oxidative weathering of upper continental crust for Early Cambrian ocean.

Reconstruction of the local depositional environment through redox

proxies, including RSE contents, V/Cr, Ni/Co, V/(V + Ni), Mo_{EF}/U_{EF}, and Re/Mo ratios, indicates that the depositional environment of the Niutitang Formation evolved from euxinic to oxic conditions. The upper core section is characterized by low TOC contents, weak RSE enrichment, and low V/Cr, Ni/Co, V/(V + Ni), Mo_{EF}/U_{EF}, and Re/Mo ratios, indicating dominantly oxic conditions. The lower core section exhibits much higher TOC contents, strong RSE enrichment, relatively high V/Cr, Ni/Co, V/(V + Ni), and Mo_{EF}/U_{EF} ratios, and low Re/Mo ratios, indicating dominantly euxinic conditions.

The Mo isotopic composition in the sedimentary succession of the YC9 drillcore exhibits a large variation, with $\delta^{98/95}$Mo values of 0.04 to 2.00‰. The upper core section is characterized by relatively low $\delta^{98/95}$Mo values of 0.18–1.27‰ (average 0.62 ± 0.42‰), while the lower section has values of 0.04–2.00‰ (average 1.10 ± 0.55‰). The upper section $\delta^{98/95}$Mo values display generally opposite trends to Mn content, negatively correlated with Mo/TOC ratios, indicating Mo fractionation associated with adsorption on Mn oxides or oxyhydroxides under oxic conditions. Lower section $\delta^{98/95}$Mo values are positively correlated with Mo/TOC ratios and negatively with Re/Mo ratios, suggesting incomplete conversion of molybdates to tetrathiomolybdates under weakly euxinic conditions. Hence, the highest $\delta^{98/95}$Mo value (2.00‰) of the lower section may represent a minimum value for contemporaneous seawater. High seawater $\delta^{98/95}$Mo ($\geq 2.00‰$) values coupled with high average Mo/TOC ratios (21 (10^{-6} g/g)/wt%) suggest extensive ocean oxygenation at ca. 520 Ma.

Supplementary data to this article can be found online at https://doi.org/10.1016/j.chemgeo.2018.08.016.

References

Algeo, T.J., Lyons, T.W., 2006. Mo–total organic carbon covariation in modern anoxic marine environments: Implications for analysis of paleoredox and paleohydrographic conditions. Paleoceanography 21, 279–298.

Algeo, T.J., Maynard, J.B., 2004. Trace-element behavior and redox facies in core shales of Upper Pennsylvanian Kansas-type cyclothems. Chem. Geol. 206, 289–318.

Algeo, T.J., Tribovillard, N., 2009. Environmental analysis of paleoceanographic systems based on molybdenum–uranium covariation. Chem. Geol. 268, 211–225.

Alves, S., Schiano, P., Allègre, C.J., 1999. Rhenium–osmium isotopic investigation of Java subduction zone lavas. Earth Planet. Sci. Lett. 168, 65–77.

Amthor, J.E., Grotzinger, J.P., Schröder, S., Bowring, S.A., Ramezani, J., Martin, M.W., Matter, A., 2003. Extinction of Cloudina and Namacalathus at the Precambrian-Cambrian boundary in Oman. Geology 31, 431.

Anbar, A.D., 2004. Molybdenum stable isotopes: Observations, interpretations and directions. Rev. Mineral. Geochem. 55, 429–454.

Anbar, A.D., Duan, Y., Lyons, T.W., Arnold, G.L., Kendall, B., Creaser, R.A., Kaufman, A.J., Gordon, G.W., Scott, C., Garvin, J., Buick, R., 2007. A whiff of oxygen before the Great Oxidation Event? Science 317, 1903–1906.

Archer, C., Vance, D., 2008. The global riverine Mo isotope flux and quantitative estimates of anoxia in the ancient global ocean. Nat. Geosci. 1, 597–600.

Arnold, G.L., Anbar, A.D., Barling, J., Lyons, T.W., 2004. Molybdenum isotope evidence for widespread anoxia in mid-Proterozoic oceans. Science 304, 87–90.

Arnold, G.L., Lyons, T.W., Gordon, G.W., Anbar, A.D., 2012. Extreme change in sulfide concentrations in the Black Sea during the Little Ice Age reconstructed using molybdenum isotopes. Geology 40, 595–598.

Asael, D., Tissot, F.L.H., Reinhard, C.T., Rouxel, O., Dauphas, N., Lyons, T.W., Ponzevera, E., Liorzou, C., Cheron, S., 2013. Coupled molybdenum, iron and uranium stable isotopes as oceanic paleoredox proxies during the Paleoproterozoic Shunga Event. Chem. Geol. 362, 193–210.

Barling, J., Anbar, A.D., 2004. Molybdenum isotope fractionation during adsorption by

manganese oxides. Earth Planet. Sci. Lett. 217, 315–329.

Barling, J., Arnold, G.L., Anbar, A.D., 2001. Natural mass-dependent variations in the isotopic composition of molybdenum. Earth Planet. Sci. Lett. 193, 447–457.

Berner, R.A., Beerling, D.J., Dudley, R., Robinson, J.M., Wildman Jr., R.A., 2003. Phanerozoic atmospheric oxygen. Annu. Rev. Earth Planet. Sci. 31, 105–134.

Brucker, R.L.P., McManus, J., Severmann, S., Berelson, W.M., 2009. Molybdenum behavior during early diagenesis: insights from Mo isotopes. Geochem. Geophys. Geosyst. 10, 258–266.

Calvert, S.E., Pedersen, T.F., 1993. Geochemistry of recent oxic and anoxic marine sediments: implications for the geological record. Mar. Geol. 113, 67–88.

Canfield, D.E., Poulton, S.W., Knoll, A.H., Narbonne, G.M., Ross, G., Goldberg, T., Strauss, H., 2008. Ferruginous conditions dominated later Neoproterozoic deep-water chemistry. Science 321, 949–952.

Canfield, D.E., Poulton, S.W., Narbonne, G.M., 2007. Late-Neoproterozoic deep-ocean oxygenation and the rise of animal life. Science 315, 92–95.

Cave, R.R., Ravizza, G.E., German, C.R., Thomson, J., Nesbitt, R.W., 2003. Deposition of osmium and other platinum-group elements beneath the ultramafic-hosted rainbow hydrothermal plume. Earth Planet. Sci. Lett. 210, 65–79.

Chen, X., Ling, H.F., Vance, D., Shields-Zhou, G.A., Zhu, M., Poulton, S.W., Och, L.M., Jiang, S.Y., Li, D., Cremonese, L., 2015. Rise to modern levels of ocean oxygenation coincided with the Cambrian radiation of animals. Nat. Commun. 6, 7.

Cheng, M., Li, C., Zhou, L., Algeo, T.J., Zhang, F., Romaniello, S., Jin, C.S., Lei, L.D., Feng, L.J., Jiang, S.Y., 2016. Marine Mo biogeochemistry in the context of dynamically euxinic mid-depth waters: a case study of the lower Cambrian Niutitang shales, South China. Geochim. Cosmochim. Acta 183, 79–93.

Cohen, A.S., 2004. The rhenium-osmium isotope system: applications to geochronological and palaeoenvironmental problems. J. Geol. Soc. 161, 729–734.

Cohen, A.S., Coe, A.L., 1999. Precise Re–Os ages of organic-rich mudrocks and the Os isotope composition of Jurassic seawater. Earth Planet. Sci. Lett. 20-28, 159–173.

Cohen, A.S., Coe, A.L., 2002. New geochemical evidence for the onset of volcanism in the Central Atlantic magmatic province and environmental change at the Triassic-Jurassic boundary. Geology 30, 267–270.

Cohen, A.S., Coe, A.L., 2007. The impact of the Central Atlantic Magmatic Province on climate and on the Sr- and Os-isotope evolution of seawater. Palaeogeogr. Palaeoclimatol. Palaeoecol. 244, 374–390.

Creaser, R.A., Sannigrahi, P., Chacko, T., Selby, D., 2002. Further evaluation of the Re-Os geochronometer in organic-rich sedimentary rocks: a test of hydrocarbon maturation effects in the Exshaw Formation, Western Canada Sedimentary Basin. Geochim. Cosmochim. Acta 66, 3441–3452.

Crusius, J., Calvert, S., Pedersen, T., Sage, D., 1996. Rhenium and molybdenum enrichments in sediments as indicators of oxic, suboxic and sulfidic conditions of deposition. Earth Planet. Sci. Lett. 145, 65–78.

Crusius, J., Thomson, J., 2000. Comparative behavior of authigenic Re, U, and Mo during reoxidation and subsequent long-term burial in marine sediments. Geochim. Cosmochim. Acta 64, 2233–2242.

Cumming, V.M., Selby, D., Lillis, P.G., 2012. Re–Os geochronology of the lacustrine Green River Formation: insights into direct depositional dating of lacustrine successions, Re–Os systematics and Paleocontinental weathering. Earth Planet. Sci. Lett. 359–360, 194–205.

Dahl, T.W., Canfield, D.E., Rosing, M.T., Frei, R.E., Gordon, G.W., Knoll, A.H., Anbar, A.D., 2011. Molybdenum evidence for expansive sulfidic water masses in ~ 750 Ma oceans. Earth Planet. Sci. Lett. 311, 264–274.

Dahl, T.W., Hammarlund, E.U., Anbar, A.D., Bond, D.P.G., Gill, B.C., Gordon, G.W., Knoll, A.H., Nielsen, A.T., Schovsbo, N.H., Canfield, D.E., 2010. Devonian rise in atmospheric oxygen correlated to the radiations of terrestrial plants and large predatory fish. Proc. Natl. Acad. Sci. U. S. A. 107, 17911.

Dickson, A.J., Cohen, A.S., 2012. A molybdenum isotope record of Eocene Thermal Maximum 2: implications for golbal ocean redox during the early Eocene. Paleoceanography 27, PA3230.

Dickson, A.J., Cohen, A.S., Coe, A.L., 2012. Seawater oxygenation during the Paleocene-Eocene Thermal Maximum. Geology 40, 639–642.

Dill, H., 1986. Metallogenesis of early Paleozoic graptolite shales from the Graefenthal Horst (northern Bavaria-Federal Republic of Germany). Econ. Geol. 81, 889–903.

Dubin, A., Peucker-Ehrenbrink, B., 2015. The importance of organic-rich shales to the geochemical cycles of rhenium and osmium. Chem. Geol. 403, 111–120.

Emerson, S.R., Huested, S.S., 1991. Ocean anoxia and the concentrations of molybdenum and vanadium in seawater. Mar. Chem. 34, 177–196.

Erickson, B.E., Helz, G.R., 2000. Molybdenum(VI) speciation in sulfidic waters: stability and lability of thiomolybdates. Geochim. Cosmochim. Acta 64, 1149–1158.

Esser, B.K., Turekian, K.K., 1993. The osmium isotopic composition of the continental crust. Geochim. Cosmochim. Acta 57, 3093–3104.

Feng, L., Li, C., Huang, J., Chang, H., Chu, X., 2014. A sulfate control on marine mid-depth euxinia on the early Cambrian (ca. 529–521 Ma) Yangtze platform, South China. Precambrian Res. 246, 123–133.

Feng, Z.Z., Peng, Y.M., Jin, Z.K., Jiang, P.L., Bao, Z.D., Luo, Z., Ju, T.Y., Tian, H.Q., Wang, H., 2001. Lithofacies palaeogeography of the Cambrian in South China. J. Palaeogeogr. 3, 1–14.

Fike, D.A., Grotzinger, J.P., Pratt, L.M., Summons, R.E., 2006. Oxidation of the Ediacaran Ocean. Nature 444, 744–747.

Goldberg, T., Strauss, H., Guo, Q., Liu, C., 2007. Reconstructing marine redox conditions for the Early Cambria'n Yangtze Platform: evidence from biogenic sulphur and organic carbon isotopes. Palaeogeogr. Palaeoclimatol. Palaeoecol. 254, 175–193.

Gordon, G.W., Lyons, T.W., Arnold, G.L., Roe, J., Sageman, B.B., Anbar, A.D., 2009. When do black shales tell molybdenum isotope tales? Geology 37, 535–538.

Greber, N.D., Siebert, C., Nägler, T.F., Pettke, T., 2012. $\delta^{98/95}$Mo values and molybdenum concentration data for NIST SRM 610, 612 and 3134: towards a common protocol for reporting Mo data. Geostand. Geoanal. Res. 36, 291–300.

Guo, Q., Shields, G.A., Liu, C., Strauss, H., Zhu, M., Pi, D., Goldberg, T., Yang, X., 2007. Trace element chemostratigraphy of two Ediacaran–Cambrian successions in South China: Implications for organosedimentary metal enrichment and silicification in the Early Cambrian. Palaeogeogr. Palaeoclimatol. Palaeoecol. 254, 194–216.

Hannah, J.L., Bekker, A., Stein, H.J., Markey, R.J., Holland, H.D., 2004. Primitive Os and 2316 Ma age for marine shale: implications for Paleoproterozoic glacial events and the rise of atmospheric oxygen. Earth Planet. Sci. Lett. 225, 43–52.

Hatch, J.R., Leventhal, J.S., 1992. Relationship between inferred redox potential of the depositional environment and geochemistry of the Upper Pennsylvanian (Missourian) Stark Shale Member of the Dennis Limestone, Wabaunsee County, Kansas, U.S.A. Chem. Geol. 99, 65–82.

Hattori, Y., Suzuki, K., Honda, M., Shimizu, H., 2003. Re-Os isotope systematics of the Taklimakan Desert sands, moraines and river sediments around the taklimakan desert, and of Tibetan soils. Geochim. Cosmochim. Acta 67, 1203–1213.

Helz, G.R., Miller, C.V., Charnock, J.M., Mosselmans, J.F.W., Pattrick, R.A.D., Garner, C.D., Vaughan, D.J., 1996. Mechanism of molybdenum removal from the sea and its concentration in black shales: EXAFS evidence. Cellular Physiology and Biochemistry International Journal of Experimental Cellular Physiology Biochemistry and Pharmacology 60, 3631–3642.

Herrmann, A.D., Kendall, B., Algeo, T.J., Gordon, G.W., Wasylenki, L.E., Anbar, A.D., 2012. Anomalous molybdenum isotope trends in Upper Pennsylvanian euxinic facies: significance for use of δ^{98}Mo as a global marine redox proxy. Chem. Geol. 324-325, 87–98.

Holland, H.D., 1979. Metals in black shales: a reassessment. Econ. Geol. 74, 1676–1680.

Horan, M.F., Morgan, J.W., Grauch, R.I., Coveney, R.M., Murowchick, J.B., Hulbert, L.J., 1994. Rhenium and osmium isotopes in black shales and Ni-Mo-PGE-rich sulfide layers, Yukon Territory, Canada, and Hunan and Guizhou provinces, China. Geochim. Cosmochim. Acta 58, 257–265.

Jaffe, L.A., Peucker-Ehrenbrink, B., Petsch, S.T., 2002. Mobility of rhenium, platinum group elements and organic carbon during black shale weathering. Earth Planet. Sci. Lett. 198, 339–353.

Jiang, S.Y., Chen, Y.Q., Ling, H.F., Yang, J.H., Feng, H.Z., Ni, P., 2006. Trace- and rare-earth element geochemistry and Pb–Pb dating of black shales and intercalated Ni–Mo–PGE–Au sulfide ores in Lower Cambrian strata, Yangtze Platform, South China. Mineral. Deposita 41, 453–467.

Jiang, S.Y., Pi, D.H., Christoph, H., Hartwig, F., Liu, Y.P., Deng, H.L., Ling, H.F., Yang, J.H., 2009. Early Cambrian ocean anoxia in South China. Nature 459, E5–E6.

Jiang, Y., Sun, M., Zhao, G., Yuan, C., Xiao, W., Xia, X., 2011. Precambrian detrital zircons in the Early Paleozoic Chinese Altai: their provenance and implications for the crustal growth of central Asia. Precambrian Res. 189, 140–154.

Jin, C.S., Chao, L.I., Peng, X.F., Cui, H., Shi, W., Zhang, Z.H., 2014. Spatiotemporal variability of ocean chemistry in the early Cambrian, South China. Sci. Sin. Terrae 57, 579–591.

Johnston, D.T., Poulton, S.W., Goldberg, T., Sergeev, V.N., Podkovyrov, V., Vorob'Eva, N.G., Bekker, A., Knoll, A.H., 2012. Late Ediacaran redox stability and metazoan evolution. Earth Planet. Sci. Lett. 335–336, 25–35.

Jones, B., Manning, D.A.C., 1994. Comparison of geochemical indices used for the interpretation of palaeoredox conditions in ancient mudstones. Chem. Geol. 111, 111–129.

Kendall, B., Creaser, R.A., Gordon, G.W., Anbar, A.D., 2009b. Re–Os and Mo isotope systematics of black shales from the Middle Proterozoic Velkerri and Wollogorang Formations, McArthur Basin, northern Australia. Geochim. Cosmochim. Acta 73, 2534–2558.

Kendall, B., Creaser, R.A., Selby, D., 2006. Re-Os geochronology of postglacial black shales in Australia: constraints on the timing of "Sturtian" glaciation. Geology 34, 729–732.

Kendall, B., Creaser, R.A., Selby, D., 2009a. ^{187}Re-^{187}Os geochronology of Precambrian organic-rich sedimentary rocks. Geol. Soc. Lond. Spec. Publ. 326, 85–107.

Kendall, B., Dahl, T.W., Anbar, A.D., 2017. The stable isotope geochemistry of molybdenum. Rev. Mineral. Geochem. 82, 683–732.

Kendall, B., Gordon, G.W., Poulton, S.W., Anbar, A.D., 2011. Molybdenum isotope constraints on the extent of late Paleoproterozoic ocean euxinia. Earth Planet. Sci. Lett. 307, 450–460.

Kendall, B., Komiya, T., Lyons, T.W., Bates, S.M., Gordon, G.W., Romaniello, S.J., Jiang, G., Creaser, R.A., Xiao, S., McFadden, K., Sawaki, Y., Tahata, M., Shu, D., Han, J., Li, Y., Chu, X., Anbar, A.D., 2015. Uranium and molybdenum isotope evidence for an episode of widespread ocean oxygenation during the late Ediacaran Period. Geochim. Cosmochim. Acta 156, 173–193.

Kendall, B., et al., 2010. Pervasive oxygenation along late Archaean Ocean margins. Nat. Geosci. 3, 647–652.

Kendall, B.S., Creaser, R.A., Ross, G.M., Selby, D., 2004. Constraints on the timing of Marinoan "Snowball Earth" glaciation by ^{187}Re-^{187}Os dating of a Neoproterozoic, post-glacial black shale in Western Canada. Earth Planet. Sci. Lett. 222, 729–740.

Kurzweil, F., Drost, K., Pašava, J., Wille, M., Taubald, H., Schoeckle, D., Schoenberg, R., 2015. Coupled sulfur, iron and molybdenum isotope data from black shales of the Teplá-Barrandian unit argue against deep ocean oxygenation during the Ediacaran. Geochim. Cosmochim. Acta 171, 121–142.

Landing, E., 2004. Precambrian–Cambrian boundary interval deposition and the marginal platform of the Avalon microcontinent. J. Geodyn. 37, 411–435.

Lehmann, B., Nägler, T.F., Holland, H.D., Wille, M., Mao, J., Pan, J., Ma, D., Dulski, P., 2007. Highly metalliferous carbonaceous shale and Early Cambrian seawater. Geology 35, 403–406.

Levasseur, S., Birck, J.L., Allègre, C.J., 1999. The osmium riverine flux and the oceanic mass balance of osmium. Earth Planet. Sci. Lett. 174, 7–23.

Li, C., Love, G.D., Lyons, T.W., Fike, D.A., Sessions, A.L., Chu, X., 2010. A stratified redox

model for the Ediacaran Ocean. Science 328, 80.

Li, C., Love, G.D., Lyons, T.W., Scott, C.T., Feng, L., Huang, J., Chang, H., Zhang, Q., Chu, X., 2012. Evidence for a redox stratified Cryogenian marine basin, Datangpo Formation, South China. Earth Planet. Sci. Lett. 331–332, 246–256.

Li, J., Jiang, X.Y., Xu, J.F., Zhong, L.F., Wang, X.C., Wang, G.Q., Zhao, P.P., 2013. Determination of platinum-group elements and Re-Os isotopes using ID-ICP-MS and N-TIMS from a single digestion after two-stage column separation. Geostand. Geoanal. Res. 38, 37–50.

Li, J., Liang, X.R., Zhong, L.F., Wang, X.C., Ren, Z.Y., Sun, S.L., Zhang, Z.F., Xu, J.F., 2014. Measurement of the isotopic composition of molybdenum in geological samples by MC-ICP-MS using a novel chromatographic extraction technique. Geostand. Geoanal. Res. 38, 345–354.

Li, J., Zhao, P.P., Liu, J., Wang, X.C., Yang, A.Y., Wang, G.Q., Xu, J.F., 2015. Reassessment of hydrofluoric acid desilicification in the Carius tube digestion technique for Re–Os isotopic determination in geological samples. Geostand. Geoanal. Res. 39, 17–30.

Li, S.R., Xiao, Q.Y., Shen, J.F., Sun, L., Liu, B., Yan, B.K., Jiang, Y.H., 2003. Rhenium-osmium isotope constraints on the age and source of the platinum mineralization in the Lower Cambrian black rock series of Hunan-Guizhou provinces, China. Sci. China. Ser. D Earth Sci. 46, 919–927.

Li, Z.X., Li, X.H., Zhou, H., Kinny, P.D., 2002. Grenvillian continental collision in South China: new Shrimp U-Pb zircon results and implications for the configuration of Rodinia. Geology 30, 163–166.

Liermann, L.J., Mathur, R., Wasylenki, L.E., Nuester, J., Anbar, A.D., Brantley, S.L., 2011. Extent and isotopic composition of Fe and Mo release from two Pennsylvania shales in the presence of organic ligands and bacteria. Chem. Geol. 281, 167–180.

Liu, Y., Liu, H.C., Li, X.H., 1996. Simultaneous precise determination of 40 trace elements in rock samples using ICP-MS. Geochimica 6, 552–558.

Ludwig, K.R., 2003. ISOPLOT, a Geochronological Toolkit for Microsoft Excel 3.00, 5. pp. 1–75.

Mao, J., Lehmann, B., Du, A., Zhang, G., Ma, D., Wang, Y., Zeng, M., Kerrick, R., 2002. Re-Os dating of polymetallic Ni-Mo-PGE-Au mineralization in Lower Cambrian black shales of South China and its geologic significance. Econ. Geol. 97, 1051–1061.

Martin, C.E., Peucker-Ehrenbrink, B., Brunskill, G.J., Symczak, R., 2000. Sources and sinks of unradiogenic osmium runoff from Papua New Guinea. Earth Planet. Sci. Lett. 183, 261–274.

McFadden, K.A., Huang, J., Chu, X., Jiang, G., Kaufman, A.J., Zhou, C., Yuan, X., Xiao, S., 2008. Pulsed oxidation and biological evolution in the Ediacaran Doushantuo Formation. Proc. Natl. Acad. Sci. U. S. A. 105, 3197–3202.

McManus, J., Berelson, W.M., Severmann, S., Poulson, R.L., Hammond, D.E., Klinkhammer, G.P., 2006. Molybdenum and uranium geochemistry in continental margin sediments: Paleoproxy potential. Geochim. Cosmochim. Acta 70, 4643–4662.

Miller, C.A., Peucker-Ehrenbrink, B., Walker, B.D., Marcantonio, F., 2011. Re-assessing the surface cycling of molybdenum and rhenium. Geochim. Cosmochim. Acta 75, 7146–7179.

Morford, J.L., Emerson, S.R., Breckel, E.J., Kim, S.H., 2005. Diagenesis of oxyanions (V, U, Re, and Mo) in pore waters and sediments from a continental margin. Geochim. Cosmochim. Acta 69, 5021–5032.

Morford, J.L., Martin, W.R., François, R., Carney, C.M., 2009. A model for uranium, rhenium, and molybdenum diagenesis in marine sediments based on results from coastal locations. Geochim. Cosmochim. Acta 73, 2938–2960.

Nägler, T.F., Anbar, A.D., Archer, C., Goldberg, T., Gordon, G.W., Greber, N.D., Siebert, C., Sohrin, Y., Vance, D., 2014. Proposal for an international molybdenum isotope measurement standard and data representation. Geostand. Geoanal. Res. 38, 149–151.

Nägler, T.F., Siebert, C., Lüschen, H., Böttcher, M.E., 2005. Sedimentary Mo isotope record across the Holocene fresh–brackish water transition of the Black Sea. Chem. Geol. 219, 283–295.

Neubert, N., Nägler, T.F., Böttcher, M.E., 2008. Sulfidity controls molybdenum isotope fractionation into euxinic sediments: evidence from the modern Black Sea. Geology 36, 775–778.

Noordmann, J., Weyer, S., Montoya-Pino, C., Dellwig, O., Neubert, N., Eckert, S., Paetzel, M., Böttcher, M.E., 2015. Uranium and molybdenum isotope systematics in modern euxinic basins: case studies from the Central Baltic Sea and the Kyllaren fjord (Norway). Chem. Geol. 396, 182–195.

Och, L.M., Shields-Zhou, G.A., 2012. The Neoproterozoic oxygenation event: environmental perturbations and biogeochemical cycling. Earth Sci. Rev. 110, 26–57.

Orberger, B., Pasava, J., Gallien, J.P., Daudin, L., Trocellier, P., 2003. Se, As, Mo, Ag, Cd, In, Sb, Pt, Au, Tl, Re traces in biogenic and abiogenic sulfides from black shales (Selwyn Basin, Yukon territories, Canada): a nuclear microprobe study. Nuclear Instruments and Methods in Physics Research 210, 441–448.

Oxburgh, R., 1998. Variations in the osmium isotope composition of sea water over the past 200,000 years. Earth Planet. Sci. Lett. 159, 183–191.

Paquay, F.S., Ravizza, G., 2012. Heterogeneous seawater $^{187}Os/^{188}Os$ during the Late Pleistocene glaciations. Earth Planet. Sci. Lett. 349-350, 126–138.

Pearce, C.R., Burton, K.W., James, R.H., Gíslason, S.R., 2010. Molybdenum isotope behaviour accompanying weathering and riverine transport in a basaltic terrain. Earth Planet. Sci. Lett. 295, 104–114.

Pearce, C.R., Cohen, A.S., Coe, A.L., Burton, K.W., 2008. Molybdenum isotope evidence for global ocean anoxia coupled with perturbations to the carbon cycle during the Early Jurassic. Geology 36, 231–234.

Pearce, C.R., Cohen, A.S., Parkinson, I.J., 2009. Quantitative separation of molybdenum and rhenium from geological materials for isotopic determination by MC-ICP-MS. Geostand. Geoanal. Res. 33, 219–229.

Pegram, W.J., Krishnaswami, S., Ravizza, G.E., Turekian, K.K., 1992. The record of sea water $^{187}Os/^{186}Os$ variation through the Cenozoic. Earth Planet. Sci. Lett. 113, 569–576.

Pegram, W.J., Turekian, K.K., 1999. The osmium isotopic composition change of Cenozoic Sea water as inferred from a deep-sea core corrected for meteoritic contributions. Geochim. Cosmochim. Acta 63, 4053–4058.

Peucker-Ehrenbrink, B., 1996. Accretion of extraterrestrial matter during the last 80 million years and its effect on the marine osmium isotope record. Geochim. Cosmochim. Acta 60, 3187–3196.

Peucker-Ehrenbrink, B., Jahn, B.M., 2001. Rhenium-osmium isotope systematics and platinum group element concentrations: loess and the upper continental crust. Geochem. Geophys. Geosyst. 2, 22–1061.

Peucker-Ehrenbrink, B., Ravizza, G., 2000. The marine osmium isotope record. Terra Nova 12, 205–219.

Peucker-Ehrenbrink, B., Ravizza, G., Hofmann, A.W., 1995. The marine $^{187}Os/^{186}Os$ record of the past 80 million years. Earth Planet. Sci. Lett. 130, 155–167.

Pi, D.H., Liu, C.Q., Shields-Zhou, G.A., Jiang, S.Y., 2013. Trace and rare earth element geochemistry of black shale and kerogen in the early Cambrian Niutitang Formation in Guizhou province, South China: Constraints for redox environments and origin of metal enrichments. Precambrian Res. 225, 218–229.

Pierson-Wickmann, A.C., Reisberg, L., France-Lanord, C., 2002. Behavior of Re and Os during low-temperature alteration: results from Himalayan soils and altered black shales. Geochim. Cosmochim. Acta 66, 1539–1548.

Poulson, R.L., Siebert, C., McManus, J., Berelson, W.M., 2006. Authigenic molybdenum isotope signatures in marine sediments. Geology 34, 617–620.

Proemse, B.C., Grasby, S.E., Wieser, M.E., Mayer, B., Beauchamp, B., 2013. Molybdenum isotopic evidence for oxic marine conditions during the latest Permian extinction. Geology 41, 967–970.

Ravizza, G., Esser, B.K., 1993. A possible link between the seawater osmium isotope record and weathering of ancient sedimentary organic matter. Chem. Geol. 107, 255–258.

Ravizza, G., Martin, C.E., German, C.R., Thompson, G., 1996. Os isotopes as tracers in seafloor hydrothermal systems: metalliferous deposits from the TAG hydrothermal area, 26° N Mid-Atlantic Ridge. Earth Planet. Sci. Lett. 138, 105–119.

Ravizza, G., Norris, R.N., Blusztajn, J., Aubry, M.P., 2001. An osmium isotope excursion associated with the late Paleocene thermal maximum: evidence of intensified chemical weathering. Paleoceanography 16, 155–163.

Ravizza, G., Paquay, F., 2008. Os isotope chemostratigraphy applied to organic-rich marine sediments from the Eocene-Oligocene transition on the West African margin (ODP Site 959). Paleoceanography 23, 977–990.

Ravizza, G., Peucker-Ehrenbrink, B., 2003. Chemostratigraphic evidence of Deccan volcanism from the marine osmium isotope record. Science 302, 1392–1395.

Ravizza, G., Turekian, K.K., 1989. Application of the ^{187}Re-^{187}Os system to black shale geochronometry. Geochim. Cosmochim. Acta 53, 3257–3262.

Ravizza, G., Turekian, K.K., 1992. The osmium isotopic composition of organic-rich marine sediments. Earth Planet. Sci. Lett. 110, 1–6.

Ravizza, G., Turekian, K.K., Hay, B.J., 1991. The geochemistry of rhenium and osmium in recent sediments from the Black Sea. Geochim. Cosmochim. Acta 55, 3741–3752.

Rimmer, S.M., 2004. Geochemical paleoredox indicators in Devonian-Mississippian black shales, central Appalachian basin (USA). Chem. Geol. 206, 373–391.

Rooney, A.D., Selby, D., Lewan, M.D., Lillis, P.G., Houzay, J.P., 2012. Evaluating Re–Os systematics in organic-rich sedimentary rocks in response to petroleum generation using hydrous pyrolysis experiments. Geochim. Cosmochim. Acta 77, 275–291.

Sahoo, S.K., Planavsky, N.J., Kendall, B., Wang, X., Shi, X., Scott, C., Anbar, A.D., Lyons, T.W., Jiang, G., 2012. Ocean oxygenation in the wake of the Marinoan glaciation. Nature 489, 546–549.

Schaefer, B.F., Burgess, J.M., 2003. Re-Os isotopic age constraints on deposition in the Neoproterozoic Amadeus Basin: implications for the "Snowball Earth". J. Geol. Soc. 160, 825–828.

Scholz, F., McManus, J., Sommer, S., 2013. The manganese and iron shuttle in a modern euxinic basin and implications for molybdenum cycling at euxinic ocean margins. Chem. Geol. 355, 56–68.

Schröder, S., Grotzinger, J.P., 2007. Evidence for anoxia at the Ediacaran-Cambrian boundary: the record of redox-sensitive trace elements and rare earth elements in Oman. J. Geol. Soc. 164, 175–187.

Scott, C., Lyons, T.W., 2012. Contrasting molybdenum cycling and isotopic properties in euxinic versus non-euxinic sediments and sedimentary rocks: refining the paleoproxies. Chem. Geol. 324–325, 19–27.

Selby, D., Creaser, R.A., 2003. Re–Os geochronology of organic rich sediments: an evaluation of organic matter analysis methods. Chem. Geol. 200, 225–240.

Sharma, M., Wasserburg, G.J., Hofmann, A.W., Butterfield, D.A., 2000. Osmium isotopes in hydrothermal fluids from the Juan de Fuca Ridge. Earth Planet. Sci. Lett. 179, 139–152.

Siebert, C., Kramers, J.D., Meisel, T., Morel, P., Nägler, T.F., 2005. PGE, Re-Os, and Mo isotope systematics in Archean and early Proterozoic sedimentary systems as proxies for redox conditions of the early Earth. Geochim. Cosmochim. Acta 69, 1787–1801.

Siebert, C., McManus, J., Bice, A., Poulson, R., Berelson, W.M., 2006. Molybdenum isotope signatures in continental margin marine sediments. Earth Planet. Sci. Lett. 241, 723–733.

Siebert, C., Nägler, T.F., Blanckenburg, F.V., Kramers, J.D., 2003. Molybdenum isotope records as a potential new proxy for paleoceanography. Earth Planet. Sci. Lett. 211, 159–171.

Siebert, C., Nägler, T.F., Kramers, J.D., 2001. Determination of molybdenum isotope fractionation by double-spike multicollector inductively coupled plasma mass spectrometry. Geochem. Geophys. Geosyst. 2, 1032.

Siebert, C., Pett-Ridge, J.C., Opfergelt, S., Guicharnaud, R.A., Halliday, A.N., Burton, K.W., 2015. Molybdenum isotope fractionation in soils: influence of redox conditions, organic matter, and atmospheric inputs. Geochim. Cosmochim. Acta 162, 1–24.

Singh, S.K., Trivedi, J.R., Krishnaswami, S., 1999. Re-Os isotope systematics in black

shales from the Lesser Himalaya: their chronology and role in the [187]Os/[188]Os evolution of seawater. Geochim. Cosmochim. Acta 63, 2381–2392.

Smoliar, M.I., Walker, R.J., Morgan, J.W., 1996. Re-Os ages of group IIA, IIIA, IVA, and IVB iron meteorites. Science 271, 1099–1102.

Steiner, M., Wallis, E., Erdtmann, B., Zhao, Y., Yang, R., 2001. Submarine-hydrothermal exhalative ore layers in black shales from South China and associated fossils - insights into a Lower Cambrian facies and bio-evolution. Palaeogeogr. Palaeoclimatol. Palaeoecol. 169, 165–191.

Taylor, S.R., McLennan, S.M., 1985. The Continental Crust: its composition and evolution, an examination of the geochemical record preserved in sedimentary rocks. J. Geol. 94, 632–633.

Tribovillard, N., Algeo, T.J., Lyons, T., Riboulleau, A., 2006. Trace metals as paleoredox and paleoproductivity proxies: an update. Chem. Geol. 232, 12–32.

Turgeon, S., Brumsack, H.J., 2006. Anoxic vs dysoxic events reflected in sediment geochemistry during the Cenomanian–Turonian Boundary Event (Cretaceous) in the Umbria–Marche Basin of central Italy. Chem. Geol. 234, 321–339.

Vine, J.D., Tourtelot, E.B., 1970. Geochemistry of black shale deposits - a summary report. Econ. Geol. 65, 253–272.

Wang, J., Chen, D., Yan, D., Wei, H., Xiang, L., 2012b. Evolution from an anoxic to oxic deep ocean during the Ediacaran–Cambrian transition and implications for bioradiation. Chem. Geol. 306–307, 129–138.

Wang, J., Li, Z.X., 2003. History of Neoproterozoic rift basins in South China: implications for Rodinia break-up. Precambrian Res. 122, 141–158.

Wang, X., Shi, X., Jiang, G., Zhang, W., 2012a. New U–Pb age from the basal Niutitang Formation in South China: implications for diachronous development and condensation of stratigraphic units across the Yangtze platform at the Ediacaran–Cambrian transition. J. Asian Earth Sci. 48, 1–8.

Wang, Z., Ma, J., Li, J., Wei, G., Chen, X., Deng, W., Xie, L., Lu, W., Zou, L., 2015. Chemical weathering controls on variations in the molybdenum isotopic composition of river water: evidence from large rivers in China. Chem. Geol. 410, 201–212.

Wen, H.J., Carignan, J., Zhang, Y.X., Fan, H.F., Cloquet, C., Liu, S.R., 2011. Molybdenum isotopic records across the Precambrian-Cambrian boundary. Geology 39, 775–778.

Wen, H.J., Fan, H.F., Zhang, Y.X., Cloquet, C., Carignan, J., 2015. Reconstruction of early Cambrian ocean chemistry from Mo isotopes. Geochim. Cosmochim. Acta 164, 1–16.

Wen, H.J., Zhang, Y.X., Fan, H.F., Hu, R.Z., 2009. Mo isotopes in the Lower Cambrian formation of southern China and its implications on paleo-ocean environment. Chin. Sci. Bull. 54, 4756–4762.

Westermann, S., Vance, D., Cameron, V., Archer, C., Robinson, S.A., 2014. Heterogeneous oxygenation states in the Atlantic and Tethys oceans during Oceanic Anoxic Event 2. Earth Planet. Sci. Lett. 404, 178–189.

Wille, M., Nägler, T.F., Lehmann, B., Schroder, S., Kramers, J.D., 2008. Hydrogen sulphide release to surface waters at the Precambrian/Cambrian boundary. Nature 453, 767–769.

Wille, M., et al., 2007. Evidence for a gradual rise of oxygen between 2.6 and 2.5 Ga from

Mo isotopes and Re-PGE signatures in shales. Geochim. Cosmochim. Acta 71, 2417–2435.

Wu, C., Zhang, M., Ma, W., Liu, Y., Xiong, D., Sun, L., 2014. Organic matter characteristic and sedimentary environment of the Lower Cambrian Niutitang shale in southeastern Chongqing. Nat. Gas Geosci. 25, 1267–1274.

Xiang, L., Schoepfer, S.D., Shen, S.Z., Cao, C.Q., Zhang, H., 2017. Evolution of oceanic molybdenum and uranium reservoir size around the Ediacaran–Cambrian transition: evidence from western Zhejiang, South China. Earth Planet. Sci. Lett. 464, 84–94.

Xu, L., Lehmann, B., Mao, J., Nägler, T.F., Neubert, N., Böttcher, M.E., Escher, P., 2012. Mo isotope and trace element patterns of Lower Cambrian black shales in South China: Multi-proxy constraints on the paleoenvironment. Chem. Geol. 318–319, 45–59.

Xu, L., Lehmann, B., Mao, J., Qu, W., Du, A., 2011. Re-Os age of polymetallic Ni-Mo-PGE-Au mineralization in Early Cambrian black shales of South China–a reassessment. Econ. Geol. 106, 511–522.

Yang, G., Hannah, J.L., Zimmerman, A., Stein, H.J., Bekker, A., 2009. Re–Os depositional age for Archean carbonaceous slates from the southwestern Superior Province: challenges and insights. Earth Planet. Sci. Lett. 280, 83–92.

Yang, J.H., Jiang, S.Y., Ling, H.F., Feng, H.Z., Chen, Y.Q., Chen, J.H., 2004. Paleoceangraphic significance of redox-sensitive metals of black shales in the basal Lower Cambrian Niutitang Formation, South China. Progress in Natural Science:Materials International 14, 152–157.

Yin, L., Li, J., Liu, J., Li, C., Sun, S.L., Liang, H.Y., Xu, J.F., 2017. Precise and accurate Re–Os isotope dating of organic-rich sedimentary rocks by thermal ionization mass spectrometry with an improved H_2O_2-HNO_3 digestion procedure. Int. J. Mass Spectrom. 421, 263–270.

Zhang, J.P., Fan, T.L., Algeo, T.J., Li, Y.F., Zhang, J.C., 2017. Paleo-marine environments of the Early Cambrian Yangtze Platform. Palaeogeogr. Palaeoclimatol. Palaeoecol. 443, 66–79.

Zhao, P.P., Li, J., Zhang, L., Wang, Z.B., Kong, D.X., Ma, J.L., 2016. Molybdenum mass fractions and isotopic compositions of International Geological Reference Materials. Geostand. Geoanal. Res. 40, 217–226.

Zhou, L., Algeo, T.J., Shen, J., Hu, Z.F., Gong, H., Xie, S., Huang, J.H., Gao, S., 2015. Changes in marine productivity and redox conditions during the Late Ordovician Hirnantian glaciation. Palaeogeogr. Palaeoclimatol. Palaeoecol. 420, 223–234.

Zhou, L., Wignall, P.B., Su, J., Feng, Q., Xie, S., Zhao, L., Huang, J., 2012. U/Mo ratios and $\delta^{98/95}$Mo as local and global redox proxies during mass extinction events. Chem. Geol. 324–325, 99–107.

Zhu, B., Becker, H., Jiang, S.Y., Pi, D.H., Fischer-Gödde, M., Yang, J.H., 2013. Re–Os geochronology of black shales from the Neoproterozoic Doushantuo Formation, Yangtze platform, South China. Precambrian Res. 225, 67–76.

Zhu, M., Zhang, J., Steiner, M., Yang, A., Li, G., Erdtmann, B., 2003. Sinian-Cambrian stratigraphic framework for shallow-to deep-water environments of the Yangtze Platform: an integrated approach. Prog. Nat. Sci. 13, 951–960.